OSBORNE, Weymar Zack. RESULTS OBTAINED FROM A STUDY OF NEGATIVE KAON INTERACTIONS IN NUCLEAR EMULSION.

The University of Oklahoma, Ph.D., 1961
Physics, nuclear

University Microfilms, Inc., Ann Arbor, Michigan

THE UNIVERSITY OF OKLAHOMA

GRADUATE COLLEGE

RESULTS OBTAINED FROM A STUDY OF NEGATIVE KAON INTERACTIONS IN NUCLEAR EMULSION

A DISSERTATION

SUBMITTED TO THE GRADUATE FACULTY

in partial fulfillment of the requirements for the degree of

DOCTOR OF PHILOSOPHY

BY

WEYMAR ZACK OSBORNE

Norman, Oklahoma

1961

RESULTS OBTAINED FROM A STUDY OF NEGATIVE KAON INTERACTIONS IN NUCLEAR EMULSION

APPROVED BY

R. A. Howard

J. Rud Nielsen

J. L. Burwell

R. B. Fowler

Arthur Bernhart

DISSERTATION COMMITTEE

ACKNOWLEDGMENTS

Professor R. A. Howard has directed this research with sensitivity and patience.

Dr. M. Teucher arranged the exposure, supervised the processing of the emulsions, and provided helpful counsel during the early stages of the work. Dr. E. J. Lofgren and the Bevatron crew made the exposure possible. Mr. James Hood exercised great skill in the design and construction of microscopes. Dr. J. R. Burwell and Mr. F. L. Miller have done confirmatory track following and participated in useful discussions.

The National Science Foundation provided an immensely helpful Predoctoral Fellowship (1958-1960).

Finally, the author owes undefinable debts to his wife and parents.

TABLE OF CONTENTS

LIST OF TABLES

LIST OF ILLUSTRATIONS

RESULTS OBTAINED FROM A STUDY OF NEGATIVE KAON INTERACTIONS IN NUCLEAR EMULSION

CHAPTER I

INTRODUCTION

Some terminology must be defined at the outset. p, n, and γ are used to denote proton, neutron, and photon, respectively. π (pion) has mass 273.3 m_e (m_e is the mass of the electron) in the positive and negative charge states and mass 264.4 m_e in the neutral charge state. The charged pion has mean life 2.56×10^{-8} sec. and the mean life of the neutral pion is $\sim 3 \times 10^{-16}$ sec. K (kaon, K-meson) has mass 966 m_e and exists in the positive, negative, and neutral charge states. The charged kaon has mean life 1.2×10^{-8} sec. and the neutral kaon may exist in either of two states having mean lives 1×10^{-10} sec. and 8×10^{-8} sec. Λ (lambda hyperon) exists only in the neutral charge state and has mass 2182.8 m_e and mean life 3.0×10^{-10} sec. Σ (sigma hyperon) exists in the positive, negative, and neutral charge states. Σ^+ has mass 2327 m_e and mean life 0.9×10^{-10} sec. Σ^- has mass 2342 m_e and mean life 1.7×10^{-10} sec. The neutral sigma

hyperon has mass 2333 m_e and an extremely short mean life--theoretical estimates yield $\sim 10^{-21}$ sec. The hyperons have been observed to decay via the modes

$$\Lambda \rightarrow p + \pi^-$$
$$\rightarrow n + \pi^\circ$$
$$\Sigma^+ \rightarrow p + \pi^\circ$$
$$\rightarrow n + \pi^+$$
$$\Sigma^- \rightarrow n + \pi^-$$
$$\Sigma^\circ \rightarrow \Lambda + \gamma .$$

Possible reaction products of negative kaon-nucleon interactions are limited to a considerable extent if one imposes the currently accepted, relevant selection rules.[1] These are energy conservation, charge conservation, baryon conservation, and strangeness conservation. The baryon number is defined to be one for all elementary particles having mass greater than or equal to that of the proton and zero for all less massive elementary particles. The strangeness number is defined for elementary particles which participate in strong interactions by

$$Q = T_3 + \tfrac{1}{2}(B + S),$$

where Q is electric charge in units of the positon charge;

---

[1]See, e.g., C. O. Beasley, Jr. and W. G. Holladay, Suppl. Nuovo Cimento 7, 77 (1958).

B is the baryon number; T_3 is the third component of isospin; and S is strangeness. No self-consistent way of including leptons in this or an analogous classification scheme has yet been found, so strangeness is said to be undefined for elementary particles which do not participate in strong interactions. Each of the four quantities, B, Q, S and T_3 is additive for aggregates of strongly interacting elementary particles, and each of them changes sign under the operation of particle-antiparticle conjugation. T_3, which has been called the "third component of isospin," may be explained by appeal to an example. The near equality of the neutron and proton masses and the fact that, aside from electromagnetic effects, the present experimental status is consistent with identical proton and neutron participation in interactions make it reasonable to think of neutron and proton as two substates of an inclusive state called "nucleon". The total isospin of such inclusive particle states is taken to be the charge multiplicity, and the third component of the isospin specifies the charge substate. From what has preceded, it is at least plausible that the mathematical context appropriate for dealing with isospin is exactly the same as that usual in the treatment of mechanical spin; this is, in fact, the case. Let U_p and U_n be wave functions for proton and neutron, respectively. With this notation the usual isospin assignments are

$$T_3 U_p = + \frac{1}{2} U_p$$

$$T_3 U_n = - \frac{1}{2} U_n$$

$$T^2 U_p = \frac{1}{2}\left(\frac{1}{2} + 1\right) U_p$$

$$T^2 U_n = \frac{1}{2}\left(\frac{1}{2} + 1\right) U_n ,$$

where T is the total isospin operator. The combination of isospins for aggregates of particles is analogous to the combination of angular momenta and, for fermions, the requirement of wave function antisymmetry under exchange of all coordinates (space, spin, and isospin) for any identical pair is just equivalent to the operation of the exclusion principle. Mention should be made of the fact that the customary isospin assignments in low-energy nuclear physics are different from those customarily made in elementary particle physics.

This classification scheme for the strongly interacting elementary particles, which is referred to as the Gell-Mann--Nishijima scheme, is completely phenomenological in that no appeal is made to an underlying theory in order to choose the appropriate assignments; rather, the assignments are made solely on the basis of consistency with the observed production and decay reactions. To refer to this assignment of quantum numbers simply as a "classification" scheme is, however,

rather unfair. Since its inception[1,2] the use of the notion of strangeness has proved to be invaluable in the design of new experiments and in the ordering of experimental results. These matters are treated at length in the admirable review articles of Dalitz[3] and Morpurgo.[4]

If the kaon kinetic energy is small, then the operation of the selection rules limits the number of sets of reaction products possible via strong interactions to only a few. Those single-nucleon reactions in which lambda hyperons may be produced by kaons at rest are

$$K^- + p \rightarrow \Lambda + \pi^0$$
$$K^- + p \rightarrow \Lambda + \pi^0 + \pi^0$$
$$K^- + p \rightarrow \Lambda + \pi^+ + \pi^-$$
$$K^- + n \rightarrow \Lambda + \pi^-$$
$$K^- + n \rightarrow \Lambda + \pi^- + \pi^0.$$

There are, of course, analogous exoergic negative kaon-multinucleon reactions in which lambdas are produced. The point is that one expects copious lambda production in the

---

[1] M. Gell-Mann, Phys. Rev. 92, 833 (1953).

[2] T. Nakano and K. Nishijima, Progr. Theoret. Phys. (Kyoto) 10, 581 (1953).

[3] R. H. Dalitz, Reports on Progress in Physics (The Physical Society, London, 1957), Vol. 20, p. 163.

[4] C. Franzinetti and G. Morpurgo, Suppl. Nuovo Cimento 6, 469 (1957).

nuclear absorption of negative kaons. It is well known that lambdas produced in nuclear interactions are occasionally bound together with various sets of nucleons to form objects called "hypernuclei" or "hyperfragments", so one expects appreciable hypernucleus production in the nuclear absorption of negative kaons. Observations made in many different laboratories have confirmed this expectation.

Sigma hyperons may be produced in the single-nucleon reactions

$$
\begin{aligned}
K^- + p &\rightarrow \Sigma^+ + \pi^- \\
&\rightarrow \Sigma^- + \pi^+ \\
&\rightarrow \Sigma^0 + \pi^0 \\
K^- + n &\rightarrow \Sigma^- + \pi^0 \\
&\rightarrow \Sigma^0 + \pi^-
\end{aligned}
$$

by a negative kaon having zero kinetic energy. As before, analogous multinucleon reactions are possible, and one expects sigma production to occur frequently in the absorption of negative kaons by nuclei.

There are two other possible reactions which should be mentioned. A negative kaon may undergo a charge-exchange scatter with a nucleus or it may simply be scattered with no change of identity.

Examination of a portion of a stack of nuclear emulsions exposed to the Bevatron K^- beam led to all of the results presented in this dissertation. Details of the experimental

techniques used are given in Chapter II. Chapter III contains a discussion of the observed characteristics of the stars caused by the negative kaon-nucleus interactions. Some simple scattering measurements were made, and the data indicate the existence of an anomalous behaviour in the elastic scattering of negative kaons; Chapter IV is devoted to this. Finally, the results of analyses of several hypernucleus decays are given in Chapter V.

CHAPTER II

EXPERIMENTAL DETAILS

Exposure and Processing of the Emulsions

The data were obtained during the systematic scanning of a stack of seventy 4 in. x 6 in. x 600 μm G-5 pellicles which had been exposed to a beam of magnetically separated negative particles of momentum 435 Mev/c at the Bevatron. The beam was composed primarily of negative pions with a small admixture of K^- mesons (or negative kaons) and negative muons. The beam entered the stack at one of the two shorter edges in a direction essentially parallel to the longer edges and the planes of the emulsion surfaces. The beam momentum was so chosen that those kaons which did not decay or interact in flight came to rest after traversing a distance in the emulsion equal to about three-fourths of the long stack dimension, i.e., the range of the kaons in the stack was about 11 cm. Just before exposure to the beam, the bottom surface of each pellicle was exposed to a carefully aligned coordinate grid consisting of 1 mm squares each of which contains a rectangular coordinate number-pair. The grid alignment was

defined by two small holes drilled through each pellicle for accommodation of corresponding pins on an aligning jig, and the exposure was accomplished by means of a process analogous to contact printing. The master grid is simply a photographic negative of a precisely scaled drawing. The negative was placed in contact with the bottom surface of each pellicle and illuminated from below in order to effect the grid exposure. Before processing, the pellicles are opaque to light whose wavelength is contained within that portion of the spectrum used for the grid exposure so only those silver halide grains at or very near (within 2 or 3 μm) the bottom surface were rendered developable. It is inevitable that some obscuration should result from this process, but this is a negligible inconvenience when compared with the resultant ease and surety in the following of tracks through adjacent emulsions. The pellicles were stacked closely together, one on top of another, in order to avoid gaps between adjacent surfaces, all the while maintaining the alignment defined by the grid exposures. The stack was then exposed to the beam. Prior to processing, except during the actual exposure, tissue paper was inserted between adjacent pellicle surfaces and the stack was misaligned. This latter procedure insures that if a track can be followed from one emulsion into an adjacent one, then it must have been produced during exposure to the beam. The grid exposure is designed to make the following of tracks through two or more single emulsions practicable; the

procedure works admirably, as, after a little practice, one can follow even tracks having minimum ionization density from one emulsion to another with little or no difficulty.

Before mounting the pellicles on glass plates the thickness of each was measured with a micrometer at a particular place so that shrinkage factors could later be determined with precision. After completion of the mounting, processing of the stack was carried out using the temperature development method and cold fixation with gradual dilution of the fixer to pure water for the washing stage. Amidol developer was used. The stack had to be processed in two different runs because of the limited capacity of the processing system. A detailed description of the procedures used in processing the stack is given in Appendix I.

Scanning Procedure

The scanning procedure used was designed specifically for the study of negative kaon decays and interactions; accordingly, a strip equal in width to one field of view was scanned across the entire emulsion at a distance of 2 cm from the beam entrance edge. The beam tracks were thus perpendicular to the longer side of the scanned strip. Since all of the particles contained in the beam were at essentially the same momentum and the mass of the kaon is more than three times as large as that of the pion, the ionization density of the tracks caused by kaons is considerably

greater than that of the tracks caused by pions; specifically, in that portion of the stack scanned to date, the pion track blob density is $178 \pm 9\ (mm)^{-1}$, and the kaon track blob density is $308 \pm 21\ (mm)^{-1}$ at the scanning strips. The ionization density of the pion tracks remains, for all practical purposes, constant throughout the dimensions of the stack. The difference in ionization density between the kaon and pion tracks is sufficiently pronounced that, with a little experience, it is possible to pick out kaon tracks by inspection with good efficiency. One is greatly assisted in doing this by the fact that the pion flux was large enough that there are several pion tracks visible at any depth in the emulsion and within any field of view; thus, a kaon track is made much more apparent by its contrast with adjacent pion tracks. The task is further simplified by the fact that the beam collimation makes appropriate the imposition of directional acceptability criteria. One still finds an appreciable number of tracks consistent with the above criteria which are not due to kaons, but almost all such tracks can easily be eliminated from consideration by following them toward the entrance edge of the stack. The majority of these "false" kaon tracks are produced by pion interactions in the region of emulsion between the entrance edge and the scanning strips and can be dismissed by inspection. At the entrance edge one may impose very strict directional acceptability criteria since the probability of a particle

having undergone upbeam scattering is negligible at this position in the stack. Only few indeed of the remaining false kaon tracks satisfy these entrance edge criteria. Those tracks which were picked up during the scanning and which satisfied the entrance edge requirements were subsequently followed downbeam through the stack until they exhibited interaction in flight, decay in flight, or stopping of the particles which caused them. In a few cases, particles underwent scattering so that they simply left the emulsion stack before one of these three eventualities occurred.

For those tracks which have thus been followed to their terminations it is only occasionally necessary to perform measurements to be sufficiently assured of the identity of the particles which caused the tracks. Confirmatory measurements are not felt necessary at all for those tracks which, having the range characteristic of beam kaons, exhibit at their terminations stars typical of K^- absorption stars. This statement is, of course, valid only for those events which are later to be included in a statistical analysis; for any individual events which are of interest because of special features, one must identify the primary particle with as much certainty as possible. Although the situation is not so clear-cut for tracks caused by particles which eventually underwent in-flight interaction, still, if the events are to be used in a later statistical analysis, the contamination of the sample by "false" kaon tracks should be unimportant

after satisfaction of the entrance edge criteria. Again, all available information should be utilized in cases where events are of individual interest. It is probably best to attempt explicit identification of the supposed primary for those events classified as apparent in-flight kaon decays.

Particle Identification Measurements

Both delta-ray counting and ionization measurements were utilized. Delta-rays are simply tracks caused by originally bound electrons which have been given sufficient energy through collision processes with another charged particle which traversed the emulsion. Ionization, as used in this context, is more difficult to define because the usage is quite loose. One is ultimately concerned with the mechanism of latent image formation for which no completely satisfactory theory exists, although the ideas of Gurney and Mott[1] are, for the most part, consistent with experiment. Basic to this development are interactions between a penetrating charged particle (or photon) and electrons bound in silver halide crystals whereby electrons are transferred from bound states to the conduction band. One speaks loosely of this process as "ionization". The tangible consequences of latent image formation are the amount and spatial distribution of silver which remains along the paths of charged particles after development. One then calls any measure of these

---

[1]R. W. Gurney and N. F. Mott, Proc. Roy. Soc. 164A, 150 (1938).

tangible track characteristics a measure of ionization.

Ionization Measurements

All ionization measurements made were based on the method of Fowler and Perkins.[1] These authors have demonstrated the validity (to within experimental fluctuations) of the relations

$$B = g \exp(-\alpha g) \qquad (2\text{-}1)$$

$$g = \frac{1}{\ell} \ln \frac{B}{H}, \qquad (2\text{-}2)$$

where B is blob density,[2] ℓ is a suitably chosen minimum admissible gap length, H is the density of gaps having length greater than ℓ, g is a parameter dependent upon ionization, and α is a parameter independent of ionization but dependent upon degree of development and resolution. They have also shown that the normalized ionization parameter, $g^* = g/g_o$, is essentially independent of the degree of development of the emulsion. Here, g_o is the (non-normalized!) ionization parameter for electron tracks having "plateau" ionization density.[3]

---

[1] P. H. Fowler and D. H. Perkins, Phil. Mag. 46, 587 (1955).

[2] A blob is silver which remains after development and which has been formed in such a way that it is completely resolvable from any neighbors that it may have.

[3] The ionization density for singly-charged particles having $E/mc^2 \geq 20$, where E is total energy and m is rest mass, appears to be constant to within a few per cent for emulsions developed together. This ionization density is called the plateau value, and the plateau grain density is about 10 per cent larger than the minimum grain density.

A plot of log g* vs. log R, where R is residual range, yields a straight line over a wide range of ionization densities for each particular variety of singly-charged particle. Optimum values of ℓ are given by $\ell g \simeq 2.5$, and O'Ceallaigh[1] has shown that ℓ must be replaced by $\ell/\cos\delta$ for tracks caused by particles which traversed the unprocessed emulsion at a dip angle δ. The parameter α is determined by making blob and gap counts on arbitrarily chosen tracks having blob densities near maximum. A large blob density is desirable simply because such tracks contain more information per unit length than do tracks having smaller blob densities. Equation (2-2) is used to compute g which is then substituted into equation (2-1) along with the measured value of B to determine α. In practice, this procedure has been carried out for several tracks in a given region of emulsion and the mean of the resulting several values of α has been used as the accepted value. In the work of this dissertation, beam pion tracks, rather than electron tracks at plateau ionization, have been used for normalization, i.e., g_o was determined for beam pion tracks which are, for all practical purposes, at minimum ionization throughout the emulsion stack. One is assured of the legitimacy of this procedure by the internal consistency and reproducibility of the final results.

---

[1] C. O'Ceallaigh, CERN Report, B. S. 11, 1954 (unpublished).

A log g* vs. log R calibration curve was constructed from measurements made on five beam kaon tracks which stopped in the emulsion and exhibited characteristic K^- absorption stars at their ends. The calibration curve was obtained by a least squares fit of the data to the equation

$$\log g_K^* = a(\log R_K) + b_K \, . \qquad (2\text{-}3)$$

The constants thus evaluated are $a = -0.478 \pm .027$ and $b_K = +1.193 \pm .035$. The data relevant to this calibration are given in Table 1.

TABLE 1

DATA FOR KAON IONIZATION CALIBRATION

Log R_K [c]	Log g_K^*
0.69412	$0.854 \pm .026$
0.93004	$0.763 \pm .031$
1.03802	$0.694 \pm .036$
1.21218	$0.628 \pm .029$
1.33575	$0.529 \pm .036$
1.50905	$0.470 \pm .035$
1.62675	$0.407 \pm .022$
1.72667	$0.386 \pm .019$
1.89503	$0.284 \pm .025$

[c] R_K is measured in mm.

Once one has constructed such a calibration curve for a known variety of singly-charged particle it is a simple matter to determine the mass of an unidentified particle that caused a track in which one is interested, provided, of course, that analogous ionization measurements may be made upon this unidentified track and provided that one is sure that the unidentified particle is singly-charged. It is well known[1,2] that for two tracks having equal ionization densities the ratio of the masses of the responsible particles is equal to the ratio of the residual ranges if the absolute values of the charges of the particles are equal. In the present context, this statement means that the mass ratio is equal to the ratio of residual ranges at equal values of g*. One immediate and useful consequence of the preceding discussion is the fact that the constant, a, which appears in equation (2-3), is independent of mass. Thus equations analogous to (2-3), but relevant to particles of different mass, differ from (2-3) only in the value of the intercept. If the masses are known, a simple calculation yields the intercepts for different types of particles; for the pion, muon, and proton they are $b_\pi = +0.930 \pm .038$, $b_\mu = +0.873 \pm .040$, and $b_p = +1.326 \pm .035$, respectively.

---

[1] A. Beiser, Revs. Modern Phys. 24, 273 (1952).

[2] L. Voyvodic, "Particle Identification with Photographic Emulsions, and Related Problems," Progress in Cosmic Ray Physics, Vol. II, ed. J. G. Wilson (Interscience Publishers, New York, 1954).

Delta-Ray Counting

This method is useful in instances where one wishes to determine the charge of a particle (usually a baryon or fragment consisting of a set of baryons bound together) responsible for a comparatively short track. Application of the method will not yield reasonable charge discrimination for tracks shorter than about 300 μm.

The conventions of Tidman, George, and Herz[1] were used in the counting of delta-rays, and the emulsion tables of Barkas and Young[2] were used to compute the expected number of delta-rays for various assumed identities of a particle of interest. The pertinent part of these emulsion tables is based on the semi-empirical work of Tidman, George, and Herz.[3] The counting conventions used contain the requirement that a blob configuration must attain a certain minimum projected displacement from the primary track in order to be eligible as a delta-ray. This minimum displacement was chosen to be 1.6 μm and calculations were carried out accordingly.

Track Length Measurements

The track length measurements and calculations were carried out by the coordinate method. An IBM 650 computer,

---

[1]D. A. Tidman, E. P. George and A. J. Herz, Proc. Phys. Soc. A 66, 1019 (1953).

[2]Walter H. Barkas and D. M. Young, University of California Radiation Laboratory Report UCRL-2579 Rev., Sept., 1954 (unpublished).

[3]Tidman, George and Herz, op. cit.

programmed for the purpose, was used in carrying out the actual computations. Details are given in Appendix II.

Range-Energy Relation

For singly-charged particles, the range-energy relation embodied in the emulsion tables of Barkas and Young[1] was used throughout this work. These tables give the correspondence between residual range and: 1. velocity, 2. kinetic energy, 3. range straggling, 4. delta-ray density, and 5. residual proper time, as well as other quantities not of direct interest here.

These tables are not reliable for use in connection with very short tracks caused by multiply-charged fragments. For such tracks, the more reliable curves given by Levi-Setti, Slater, and Telegdi[2] have been used.

Angle Measurements

In the analysis of observed events one frequently uses the conservation of momentum, so it is necessary to have available some means for determining the directions of the momenta involved or, equivalently, the directions of the corresponding tracks. One convenient method consists of determining relevant direction cosines by means of direct measurement of coordinate differences.

---

[1] Barkas and Young, op. cit.

[2] R. Levi-Setti, W. E. Slater, and V. L. Telegdi, Suppl. Nuovo Cimento 10, 68 (1958).

The direction cosine determinations were accomplished with the aid of a Leitz screw micrometer eyepiece (code word OKNOR) which had previously been calibrated with a standard stage micrometer. The micrometer eyepiece is designed for the precise measurement of displacements of the order of a few microns in the focal plane of the microscope. At the binocular width chosen (62 on Leitz binocular head scale) and with the objective used (Koristka 100X flourite oil immersion) 1000 micrometer drum divisions correspond to $31.72 \pm .24$ μm in emulsion. The micrometer eyepiece was inserted in the right side of the binocular head and the left side was covered to avoid distraction.

CHAPTER III

CHARACTERISTICS OF THE KAON INTERACTIONS

Each kaon track may exhibit graphic evidence of one of four possible histories for the generative kaon. The primary particle may have decayed in flight, interacted in flight with an emulsion nucleus, interacted at rest, or simply left the emulsion stack before one of these three eventualities occurred. Not all of the kaon-nucleus interactions caused stars with visible product prongs. This result is expected in view of the fact that some negative kaon-proton reactions have only neutral products (see Chapter I). The observations show, however, that a relatively small proportion of the kaon-nucleus interactions did indeed yield only neutral products.

Certain criteria were established for categorization of the events found during the following of tracks. For an event to be classified as an at-rest star there must be at least one visible product prong at the end of the primary track, and the primary track must have the appearance typical of tracks caused by particles which came to rest in the

emulsion. The decision as to whether a track does, or does not, have this appearance is a subjective one based largely upon experience, and it is estimated that the method is not discriminatory within the last 1 mm of a kaon track. A kaon has about 10 Mev of kinetic energy at a residual range of 1 mm. An event was classified as a zero-prong, at-rest interaction (K_ρ) provided that the primary track had the length and appearance typical of kaon tracks ending in at-rest stars and provided that there was no visual evidence of reaction products at the end of the primary track. Tentative in-flight decays are characterized by an obvious change in direction of the track coincident with a change in ionization from denser to lighter at the decay vertex. This vertex must be completely "clean", i.e., free of associated blobs or low-energy electron tracks, and it must be apparent that the primary particle was still in flight at the decay point. The in-flight stars with visible products include all events for which it was clear that the primary was in flight immediately before the interaction and for which there is visible evidence of a nuclear interaction, i.e., one or more product prongs due to heavy particles or one light product prong with a "non-clean" vertex. Some kaon tracks simply disappeared at points where the ionization density is such that the primary particle must have had a large velocity. These events, having no visible product prongs, were classified as zero-prong, in-flight interactions. A few events were observed which were apparently

kaon-nucleus interactions from which the kaons were re-emitted. These have not been included among the in-flight stars.

Eleven emulsions (#19-#25, #30-#33) were scanned completely and all of the kaon tracks followed; this gave a total of 292 events. The numbers of events belonging to the previously defined categories are:

At-rest stars	165
Zero-prong, at-rest interactions. . .	28
In-flight stars	76
Zero-prong, in-flight interactions. .	8
In-flight decays.	15.

Each prong originating in a kaon star and not classified as light (g* less than about 2.3) was followed up to the point where the generative particle came to rest, decayed in flight, underwent an in-flight interaction, or left the emulsion stack. Only a few of the prongs classified as light were followed. The ideal end result of this procedure is the specific identification of each of the charged products originating in a kaon-nucleus interaction. Unfortunately, this end is unrealizable in practice. The best one can do without making detailed measurements upon each track is to establish certain criteria for the classification of the product prongs.

Prongs caused by π^+ and π^- are quite easy to recognize, provided the generative particle stopped in the stack. The π^+ tracks exhibit graphic evidence of the characteristic decay

$$\pi^+ \rightarrow \mu^+ + \nu$$

at their ends. The π^- tracks usually have pion absorption stars at their ends, although some of the pion absorptions gave no visible products. Still, one has no difficulty if the track is longer than about 1 mm because this is enough to identify visually the parent particle as a light meson (pion or muon). Since muons do not participate in strong interactions, one is left with only the one alternative. All light prongs which leave the stack or which have not been followed have been tentatively classified as $\pi^\pm$ tracks. The notation, $\pi^\pm$, indicates that the charge of the generative particle is undetermined.

Those prongs which have been classified as

$$\Sigma^+ \rightarrow p + \pi^\circ$$

consist of a Σ^+ track with a proton track having the correct range (about 1.6 mm) originating at its end. The decay vertex was required to be completely clean. Each prong which had the appearance of a stopping proton, but with a track having near minimum ionization originating at its end, has been put in the

$$\Sigma^+ \rightarrow n + \pi^+$$

category; again, the decay vertex was required to be clean. A typical

$$\Sigma^\pm \rightarrow n + \pi^\pm$$

prong consists of a track due to a heavy particle, obviously not at rest, which changes discontinuously to a track having

minimum ionization. The ionization change will, in general, be accompanied by a change in direction and the decay vertex must be clean. All prongs caused by particles of baryonic mass which end in secondary stars having only prongs due to protons or nuclear fragments have been placed in the Σ^- or H (hypernucleus) category. Finally, all prongs which end in secondary stars typical of mesonic hypernucleus decays have been classified as H events.

Stars Caused by At-Rest Kaons

The classification numbers for prongs caused by unstable particles originating in at-rest kaon-nucleus interactions are given in Table 2.

TABLE 2

UNSTABLE PRONG CLASSIFICATIONS FOR ALL AT-REST STARS

Prong Classification	Number Observed
π^+	0
π^-	7
$\pi^\pm$	66
$\Sigma^+ \rightarrow p + \pi^\circ$	2
$\Sigma^+ \rightarrow n + \pi^+$	2
$\Sigma^\pm \rightarrow n + \pi^\pm$	6
Σ^- or H	15
H	2

These data have also been collated for those at-rest stars exhibiting visible evidence of charged pion emission and for those with no visible evidence of charged pion emission. The former data are given in Table 3 and the latter in Table 4.

TABLE 3

UNSTABLE PRONG CLASSIFICATIONS FOR AT-REST STARS HAVING ONE CHARGED PION PRONG EACH

Prong Classification	Number Observed
$\Sigma^+ \rightarrow p + \pi^o$	2
$\Sigma^+ \rightarrow n + \pi^+$	0
$\Sigma^\pm \rightarrow n + \pi^\pm$	4
Σ^- or H	8
H	1

TABLE 4

UNSTABLE PRONG CLASSIFICATIONS FOR AT-REST STARS HAVING ONLY PRONGS DUE TO BARYONS

Prong Classification	Number Observed
$\Sigma^+ \rightarrow p + \pi^o$	0
$\Sigma^+ \rightarrow n + \pi^+$	2
$\Sigma^\pm \rightarrow n + \pi^\pm$	2
Σ^- or H	7
H	1

All prongs apparently caused by stable particles were, of course, recorded along with the prongs caused by unstable particles. It was thus possible to arrive at total prong-number frequency distributions. These are given in Tables 5, 6, and 7.

TABLE 5

PRONG-NUMBER FREQUENCY DISTRIBUTION FOR ALL AT-REST STARS

Prong Number	Number of Stars
1	34
2	37
3	46
4	28
5	12
6	5
7	2
8	1
	165

TABLE 6

PRONG-NUMBER FREQUENCY DISTRIBUTION FOR AT-REST STARS HAVING ONE CHARGED PION PRONG EACH

Prong Number	Number of Stars
1	12
2	24

TABLE 6--Concluded

Prong Number	Number of Stars
3	18
4	13
5	3
6	1
7	2
	73

TABLE 7

PRONG-NUMBER FREQUENCY DISTRIBUTION FOR AT-REST STARS HAVING ONLY PRONGS DUE TO BARYONS

Prong Number	Number of Stars
1	22
2	13
3	28
4	15
5	9
6	4
7	0
8	1
	92

Discussion

Several detailed studies of negative kaon interactions and decays are available in the literature.[1-9] Those cited contain references to earlier works.

The results obtained here for the at-rest stars have been compared with those of the Bern group.[10,11] Two directly observable quantities--namely, observed frequency of charged pion emission and observed frequency of hyperon emission--are amenable to comparison. The relevant quantities are given in Table 8. The deviations quoted for the charged pion frequencies correspond to confidence limits at a confidence

---

[1] E. Lohrmann, et al., Nuovo Cimento 7, 163 (1958).

[2] Y. Eisenberg, et al., Nuovo Cimento 8, 663 (1958).

[3] Y. Eisenberg, et al., Nuovo Cimento 9, 745 (1958).

[4] Y. Eisenberg, et al., Nuovo Cimento 11, 351 (1958).

[5] M. Nikolic, et al., Helv. Phys. Acta 3, 221 (1960).

[6] W. Koch, et al., Helv. Phys. Acta 3, 237 (1960).

[7] K^--Collaboration, Part I, Nuovo Cimento 13, 690 (1959).

[8] K^--Collaboration, Part II, Nuovo Cimento 14, 315 (1959).

[9] K^--Collaboration, Part III, Nuovo Cimento 15, 873 (1959).

[10] Nikolic, et al., op. cit.

[11] Koch, et al., op. cit.

TABLE 8

COMPARISON OF RESULTS FOR AT-REST STARS

Star Type	Source	Observed Frequencies: Charged Pion	Observed Frequencies: Hyperon
All	This work	$0.430^{+.058}_{-.051}$	0.164
	Bern	$0.382^{+.021}_{-.020}$	0.175
With charged pion	This work		0.211
	Bern		0.214
Without charged pion	This work		0.120
	Bern		0.152

level of 68 per cent, and it has been assumed that the observed charged pion numbers belong to Poisson distributions.[1,2,3]

The reliability of the criteria used to choose $\pi^{\pm}$ prongs deserves elaboration. The members of the Bern group[4,5]

---

[1] M. G. Kendall, The Advanced Theory of Statistics, Vol. 2 (New York: Hafner Publishing Co., 1951), Chapter 19.

[2] C. A. Bennett and N. L. Franklin, Statistical Analysis in Chemistry and the Chemical Industry (New York: John Wiley and Sons, 1954), Chapter 9.

[3] E. C. Molina, Poisson's Exponential Binomial Limit (New York: D. Van Nostrand Co., 1942).

[4] Nikolic, et al., op. cit.

[5] Koch, et al., op. cit.

have measured the energy spectra of sigma hyperons and protons emitted from their sample of at-rest interactions. The estimated minimum energy corresponding to proton or charged sigma tracks that could have been included in the $\pi^{\pm}$ category of this work is 180 Mev. This information, together with the published energy spectra, allows one to conclude that at most two of the tracks classified as $\pi^{\pm}$ could have been due to baryons. Thus, a total of 71 charged pions has been used in computing the corresponding frequency for this work. The difference in the charged pion frequencies given in Table 8 is probably real, and reflects a small difference in the scanning efficiencies. It should be emphasized that both of these frequencies must be looked upon as lower bounds since a scanning efficiency of 100 per cent is probably not attainable.

All pairs of observed hyperon frequencies are felt to be in good agreement.

In-Flight Stars

The presentation of the data is exactly analogous to that for the at-rest stars. The classification numbers for prongs caused by unstable particles are given in Tables 9, 10, and 11, and the total prong-number frequency distributions are given in Tables 12, 13, and 14.

TABLE 9

UNSTABLE PRONG CLASSIFICATIONS FOR ALL IN-FLIGHT STARS

Classification	Number Observed
π^+	2
π^-	2
$\pi^\pm$	28
$\Sigma^\pm \rightarrow n + \pi^\pm$	5
Σ^- or H	10
H	3

TABLE 10

UNSTABLE PRONG CLASSIFICATIONS FOR IN-FLIGHT STARS HAVING ONE CHARGED PION PRONG EACH

Classification	Number Observed
$\Sigma^\pm \rightarrow n + \pi^\pm$	3
Σ^- or H	4
H	1

TABLE 11

UNSTABLE PRONG CLASSIFICATIONS FOR IN-FLIGHT STARS HAVING ONLY PRONGS DUE TO BARYONS

Classification	Number Observed
$\Sigma^{\pm} \rightarrow n + \pi^{\pm}$	2
Σ^{-} or H	6
H	2

TABLE 12

PRONG-NUMBER FREQUENCY DISTRIBUTION FOR ALL IN-FLIGHT STARS

Prong Number	Number of Stars
1	9
2	18
3	15
4	12
5	13
6	5
7	1
8	0
9	3
	76

TABLE 13

PRONG-NUMBER FREQUENCY DISTRIBUTION FOR IN-FLIGHT STARS HAVING ONE CHARGED PION PRONG EACH

Prong Number	Number of Stars
1	1
2	11
3	7
4	3
5	6
6	3
7	1
	32

TABLE 14

PRONG-NUMBER FREQUENCY DISTRIBUTION FOR IN-FLIGHT STARS HAVING ONLY PRONGS DUE TO BARYONS

Prong Number	Number of Stars
1	8
2	7
3	8
4	9
5	7
6	2
7	0
8	0
9	3
	44

The results have again been compared with those of the Bern[1] group. The observed charged pion and hyperon frequencies are given in Table 15. As before, the quoted deviations

TABLE 15

COMPARISON OF RESULTS FOR IN-FLIGHT STARS

Source	Frequency	
	Charged Pion	Hyperon
This work	$0.421^{+.089}_{-.074}$	$0.237^{+.070}_{-.055}$
Bern	$0.254^{+.030}_{-.026}$	$0.147^{+.023}_{-.020}$

correspond to confidence limits for the 68 per cent level of confidence.

It is apparent that the data from the two different sources are not in agreement. A comparison of Table 15 with Table 8 shows that the observed charged pion and hyperon frequencies obtained in this work for the two types (in-flight and at-rest) of stars are essentially in agreement; this is not the case for the observed Bern frequencies. This fact suggests a possible resolution of the discrepancy. A contamination of a sample of K^- interactions in flight with π^- interactions in flight would certainly depress the

[1] Y. Eisenberg, et al., Nuovo Cimento 9, 745 (1958).

observed charged pion and hyperon emission frequencies. The disagreement of the in-flight and at-rest Bern frequencies is consistent with such a contamination.

An Event of Particular Interest

One of the kaon at-rest stars (K69-22) has one prong which was caused by a Σ^-, a second prong probably due to a proton, and a third prong most probably caused by a π^-. According to the list of reactions given in Chapter I, it is impossible that a π^- and Σ^- be produced in a negative kaon interaction with only one nucleon. Simultaneous π^- and Σ^- production could occur in kaon-multinucleon reactions such as

$$K^- + (2n) \rightarrow \pi^- + \Sigma^- + p$$

or in sequences of reactions such as

$$K^- + n \rightarrow \Sigma^- + \pi^0$$
$$\pi^0 + n \rightarrow \pi^- + p$$

and

$$K^- + n \rightarrow \pi^- + \Sigma^0$$
$$\Sigma^0 + n \rightarrow \Sigma^- + p .$$

Whether or not simultaneous π^- and Σ^- production does occur in the nuclear absorption of negative kaons has been an unsettled question up to now.[1] Aside from its

---

[1] J. Sacton, Nuovo Cimento 18, 266 (1960).

intrinsic interest, it is important that this question be answered for another reason. Often it is impossible to differentiate between stars caused by the non-mesonic decay of hypernuclei and stars caused by the nuclear absorption of Σ^- hyperons. In cases where the indeterminate Σ^- or hypernucleus has been produced in association with a π^- in a kaon absorption, some workers have assumed that the indeterminate prong was due to a hypernucleus solely on the basis of the coexistence of an identified π^- prong. This criterion can, at best, be only approximately valid if the event to be described here has been correctly interpreted.

Description of the Event and Results of Measurements

The event consists of four connected stars. The primary star (S-1) was caused by the nuclear absorption of a negative kaon; one secondary star (S-2) was caused by a Σ^-; the other secondary star (S-3) was probably due to a π^-; and the tertiary (secondary to S-2) star (S-4) is probably an example of the mesonic, at-rest decay of a light hypernucleus. The identity of the primary particle was verified directly by ionization measurements--the measured value of g* at a residual range of 62 mm is 2.25, and the value expected for a kaon track at this residual range is $2.17 \pm .12$.

Product prong lengths, etc., for S-1, S-2, and S-4 are given in Tables 16, 17, and 18, respectively.

TABLE 16

DATA FOR S-1

Prong	Length	Generative Particle	Comments
1	~300 μm	Σ^-	Ends in S-2
2	~5 mm	Probably p	Stable
3	17.43 mm	π^-	Ends in S-3

TABLE 17

DATA FOR S-2

Prong	Length	Generative Particle	Comments
A	~10 μm	?	Stable
B	~250 μm	?	Stable
C	1.065 mm	$_{\Lambda}H^3$ or $_{\Lambda}H^4$	Ends in S-4

TABLE 18

DATA FOR S-4

Prong	Length	Generative Particle	Comments
a	9.1 ± 1.4 μm	He^3 or He^4	
b	> 19.47 mm	π^-	Leaves stack before stopping. The product prongs are co-linear to within the errors of measurement.

S-3 has only a large blob and one short (4 μm) product prong.

The key to interpretation of this event is the simple observation that a tertiary star does in fact exist. For the kinetic energies relevant here, the only known kaon-nucleus interaction products which could conceivably give rise to a tertiary star are Λ and Σ^-. The former can do so via the sequence

$$\text{Hypernucleus} \longrightarrow \text{Nucleons} + \pi^- + Q$$

$$\pi^- + \text{Nucleus} \longrightarrow \text{Nucleons} + Q$$

and the latter via the sequence

$$\Sigma^- + \text{Nucleus} \longrightarrow \text{Hypernucleus} + \text{Nucleons} + Q$$

$$\text{Hypernucleus} \longrightarrow \text{Decay Products} + Q$$

The first possibility can be eliminated on the basis that prong C, which interconnects S-2 and S-4, simply doesn't look like a track caused by a stopping pion. Because a pion has small mass, it undergoes a great deal of multiple scattering near the end of its range and a pion track exhibits a noticeable change in ionization over its last 1 mm. Prong C does not have these characteristics; rather, it looks like a track caused by a heavy particle which came to rest. The argument that S-4 and prong C are consistent with either of the interpretations

$$_{\Lambda}H^3 \longrightarrow He^3 + \pi^-$$

$$_{\Lambda}H^4 \longrightarrow He^4 + \pi^-$$

will be given in Chapter V (event H4).

As a check, ionization measurements were made on prong 3 (originates in S-1). These measurements did not agree with the expected values derived from the kaon calibration curve and the known kaon-pion mass ratio. This strongly indicated that the method used to derive an expected pion log g* vs. log R curve from the measured kaon calibration curve does not give reliable results. Further ionization measurements were then made on a track known from other reasons to be due to a π^-. These further measurements also did not agree with the values derived from the kaon calibration curve. The results are summarized in Table 19. These data show

TABLE 19

IONIZATION MEASUREMENTS FOR PIONS

	g*		
Residual Range	Prong 3	Identified Pion Track	Value Derived from Kaon Calibration
3.16 mm	$4.17 \pm .44$	$4.17 \pm .45$	$4.91 \pm .15$
6.97 mm	$2.76 \pm .30$	$2.75 \pm .30$	$3.37 \pm .13$
9.00 mm		$2.35 \pm .26$	$2.98 \pm .12$

clearly that a systematic deviation of the measured g* values from the derived values does exist. Also, the agreement of the measured values for prong 3 and the identified pion track show that prong 3 was probably caused by a pion. The

extreme closeness of this agreement is undoubtedly fortuitous. Since there is evidence of an interaction at the end of prong 3, one concludes that it must have been caused by a π^-.

It should be noted that a possible alternative interpretation exists. It is conceivable that a

$$\pi^+ \rightarrow \mu^+ + \nu$$

decay occurred at some point of prong 3, and that the resultant μ^+ underwent a large scatter 4 μm before the end of its range. If, then, a random large blob happened to coincide with the scatter vertex after emulsion processing, the end portion of prong 3 could have just the appearance observed. This alternative interpretation is quite improbable, however, because nowhere along prong 3 is there any graphic evidence of a decay and the probability of coincidence of a large blob and scatter vertex is small.

CHAPTER IV

SCATTERING OBSERVATIONS

Early during the process of following the kaon tracks picked up at the scanning strips it seemed that an unreasonably large proportion of the tracks exhibited two or more large-angle (greater than about 5°) scatters. Because of this suspicion, relevant data were recorded for the last 183 kaon tracks followed. Each discontinuous change of direction estimated visually to be greater than or equal to 5° was recorded along with the grid coordinates of the scatter vertex.

In the analysis of the data, each kaon track was divided into segments according to residual range. For those tracks which ended in in-flight interactions or in-flight decays the residual range was, of course, not directly observable. However, the mean range of beam kaons in the stack, determined to be 110 mm from those kaon tracks which ended in at-rest stars, was used to arrive at probable residual ranges for tracks caused by kaons that did not come to rest. The kaon tracks contained within each residual range interval were segregated according to whether they did (type II) or did

not (type I) show at least one large-angle scatter upbeam from the interval. Finally, mean free paths for scatters of 5° or more were calculated for the two classes of kaons which entered each interval. The results are given in Table 20. The overall mean free path for scatters of 5° or more is $187\ ^{+43.3}_{-35.2}$ mm for the residual range interval 60 mm < R < 90 mm. All deviations given so far in this chapter correspond to the standard 68 per cent level of confidence. The interval #1 mean free paths for the two types of kaon tracks are in complete agreement, just as one would expect. Conversely, there exists a surprisingly large disagreement between the interval #2 mean free paths for the two types of kaon tracks. Not only do the means differ a great deal, but the adjacent confidence limits miss overlap by 10 mm. This disagreement can be expressed in another form. If one assumes that the type II tracks should yield the same mean free path as the type I tracks then the expected number of scatters for type II in interval #2 is $5\ ^{+3.4}_{-2.2}$. The observed number is 12.

One other fact is worth noting. Of the 183 kaon tracks included in the scattering observations, 105 of them ended in at rest stars and 25 of these exhibited at least two scatterings of 5° or more. Four

$$\Sigma^{\pm} \rightarrow n + \pi^{\pm}$$

prongs were observed in connection with the 105 at-rest stars. Three of the four $\Sigma^{\pm}$ originated in at-rest stars caused

TABLE 20

RESULTS OF SCATTERING OBSERVATIONS

			Kaons without Upbeam Scatter (Type I)			Kaons with Upbeam Scatter (Type II)		
Interval	Residual Range Limits	Energy Limits	Total Track Length Scanned	Mean Free Path		Total Track Length Scanned	Mean Free Path	
# 1	15 mm 40 mm	50.1 Mev 91.7 Mev	2451 mm	88	+20.4 -16.2 mm	1183 mm	91	+34.2 -24.3 mm
# 2	40 mm 60 mm	91.7 Mev 112.1 Mev	2471 mm	137	+41.8 -31.4 mm	703 mm	59	+23.2 -16.1 mm

by kaons which had previously undergone at least two scatters of 5° or more.

The significance of the data contained in this chapter is certainly open to question because of poor statistics. The scattering observations are, however, sufficiently indicative of anomalous behaviour to warrant further and more careful investigation. If the anomaly should prove to be real, it could be occasioned by the existence of two fundamentally different kinds of kaons or by the existence of one or more excited states for the kaon. The former seems the more palatable of these two alternatives.

CHAPTER V

THE ANALYSIS OF SEVERAL HYPERNUCLEUS DECAYS

It was mentioned in Chapter I that lambda hyperons produced in nuclear interactions are occasionally bound together with sets of nucleons to form objects known as hypernuclei. These may decay via a mesonic mode

$$\text{Hypernucleus} \longrightarrow \pi^- + \text{Nucleons} + Q$$

or a non-mesonic mode

$$\text{Hypernucleus} \longrightarrow \text{Nucleons} + Q.$$

Of these modes, the mesonic is generally much simpler to analyze because the resultant pion track is usually identifiable by inspection.

The results of analyses of five mesonic hypernucleus decays are given in this chapter. Four of the decays occurred with the hypernucleus at rest and the other while the hypernucleus was in flight.

It is convenient to state at this point that a revised range-energy relation[1] has been used in making the hypernucleus analyses. This revision differs only slightly from the

---

[1] W. H. Barkas, Nuovo Cimento 8, 201 (1958).

emulsion tables of Barkas and Young[1] and the difference is insignificant for all work described in preceding chapters. The lambda mass of 1115.55 ± .15 Mev/c^2 given by Lodge et al.[2] was adopted.

Event H1

The event consists of a primary track which ends in a star having two product prongs. The track of the primary will be referred to as track A and the two product prongs as track B and track C. Measured quantities are given in Table 21.

TABLE 21

DATA FOR EVENT H1

Track	Length	Dip Angle	Remarks
A	2.64 mm	-	Originates in kaon in-flight star.
B	8.6 ± .3 μm	$+8.7^\circ \pm 2.8^\circ$	-
C	39.17 ± .021 mm	$-6.1^\circ \pm 1.7^\circ$	Ends in typical pion absorption star having two product prongs.

[1] Barkas and Young, op. cit.

[2] J. Lodge, et al., Nuovo Cimento 18, 147 (1960).

Tracks B and C are colinear to within the errors. The azimuthal angles were checked by aligning one axis of a cross-hair graticule along track C and then seeing that track B and the extension of track C coincide. Since track C has the appearance of a light meson track and ends in a typical pion absorption star it must have been caused by a π^-. The kinetic energy and momentum of the pion at emission were, respectively, $52.22 \pm .35$ Mev and $131.57 \pm .56$ Mev/c. Conservation of momentum and the assumption that the primary decayed at rest imply that particle B had emission momentum equal in magnitude to that of the pion. The curves given by Levi-Setti, Slater, and Telegdi[1] then show that particle B could only have been He^3, He^4, or He^6, with He^4 yielding the best agreement between measured and expected ranges. The most likely interpretation of the event is thus

$$_{\Lambda}H^4 \longrightarrow He^4 + \pi^-$$

at rest. For this interpretation, the lambda binding energy, defined by

$$B_{\Lambda} = M_{\Lambda} + M' - E_B - E_C$$

M_{Λ} = Rest energy of lambda

M' = Rest energy of H^3

E_B = Total energy of He^4 at emission

E_C = Total energy of π^- at emission,

is $2.95 \pm .38$ Mev. The interpretation

---

[1] Levi-Setti, Slater, and Telegdi, op. cit.

$$_{\Lambda}H^{3} \longrightarrow He^{3} + \pi^{-}$$

leads to non-conservation of energy and the system H^5 cannot be bound[1] so the first interpretation given is unique.

The lambda binding energy for $_{\Lambda}H^{4}$ obtained here is in good agreement with the weighted average value of 2.30 $\pm$.21 Mev given in the 1958 world-wide hypernucleus survey of Levi-Setti, Slater, and Telegdi.[2,3] The errors given in this chapter include shrinkage factor uncertainties and uncertainties arising from range straggling. The emulsions were assumed to have the normal density 3.815 g/cc.

Event H2

Three products originated in this hypernucleus decay. The primary track will be referred to as track A and the product prongs as tracks B, C, and D. The track lengths are given in Table 22.

The results of the direction measurements are most conveniently expressed as unit vectors in the coordinate system defined by the microscope. The unit vectors along the product prongs are

---

[1]The interpretation

$$_{\Lambda}H^{6} \longrightarrow He^{6} + \pi^{-}$$

and the assumption that the "binding energy" of H^5 is zero lead to B_{Λ} = 12 Mev, an unreasonably large value.

[2]Levi-Setti, Slater, and Telegdi, op. cit.

[3]These authors adopted a different lambda mass so their quoted value has been corrected accordingly to yield the number given above.

TABLE 22

DATA FOR EVENT H2

Track	Length	Remarks
A	50.6 ± 1.0 μm	Originates in kaon in-flight star.
B	72.9 ± 1.0 μm	
C	$3.9 \pm .3$ μm	
D	$13.49 \pm .051$ mm	Ends in typical pion absorption star having one product prong.

$\hat{B} = -(0.866 \pm .009)\hat{i} + (0.432 \pm .009)\hat{j} - (0.251 \pm .022)\hat{k}$

$\hat{C} = (0.903 \pm .038)\hat{i} + (0.167 \pm .040)\hat{j} + (0.407 \pm .076)\hat{k}$

$\hat{D} = -(0.692 \pm .008)\hat{i} - (0.641 \pm .007)\hat{j} - (0.331 \pm .016)\hat{k}$,

where the letters denoting the vectors correspond to the prong designations. In order to determine whether or not the three product prongs are coplanar, the quantity

$$\left(\frac{\hat{B} \times \hat{D}}{|\hat{B} \times \hat{D}|} \right) \cdot \hat{C} = 0.058 \pm .073$$

was computed. This is just the cosine of the angle between prong C and the normal to the plane of prongs B and D. It is apparent that the three product prongs are indeed coplanar to within the measurement uncertainty. It will thus be assumed in the following analysis that there were only three products of the hypernucleus decay.

Track D is identifiable by inspection as that of a π^-. The kinetic energy and momentum of the pion at emission

were, respectively, 27.63 ± .20 Mev and 92.09 ± .26 Mev/c. The assumption that particle B was a proton leads to an emission kinetic energy of 2.90 ± .05 Mev and an emission momentum of 73.79 ± .56 Mev/c. With this assumption, the residual momentum for particles D and B is

$$\vec{P}_R = (139.4) \left[- (0.916 \pm .012)\hat{i} - (0.195 \pm .007)\hat{j} - (0.352 \pm .014)\hat{k} \right] ,$$

where

$\vec{P}_R = \vec{P}_B + \vec{P}_D$,

$\vec{P}_B$ = Momentum of particle B at emission,

$\vec{P}_D$ = Momentum of particle D at emission,

and

$\vec{P}_R$ has been expressed in Mev/c.

$\vec{P}_R$ and $\hat{C}$ are colinear to within the uncertainties. If one assumes that particle B was a deuteron, this results in

$$\vec{P}_R = (177.6) \left[- (0.939 \pm .014)\hat{i} - (0.041 \pm .008)\hat{j} - (0.340 \pm .016)\hat{k} \right]$$

and so in non-colinearity of $\vec{P}_R$ and $\hat{C}$. The assumption that particle B was a yet more massive nucleus would only make matters worse. Momentum conservation thus leads to the unique identification of particle B--it was a proton. Conservation of momentum also implies that particle C had a momentum of 139.4 ± 1.24 Mev/c at emission. Either of the identities

Li^6 and Li^7 is consistent with this momentum and the measured range of track C. The first leads to the interpretation

$$_{\Lambda}Li^7 \longrightarrow \pi^- + p + Li^6$$

$$B_{\Lambda} = 5.45 \pm .37 \text{ Mev}$$

and the second to

$$_{\Lambda}Li^8 \longrightarrow \pi^- + p + Li^7$$

$$B_{\Lambda} = 5.69 \pm .37 \text{ Mev.}$$

Each of these interpretations is consistent with the measurements so the analysis cannot provide a unique interpretation.

Event H3

The hypernucleus decay caused two visible product prongs. The track lengths are given in Table 23, wherein track A denotes the primary track and tracks B and C the product prongs. The measured unit vectors along tracks B and C are

$$\hat{B} = -(0.457 \pm .011)\hat{i} - (0.339 \pm .010)\hat{j} + (0.822 \pm .056)\hat{k}$$

$$\hat{C} = (0.348 \pm .007)\hat{i} + (0.458 \pm .008)\hat{j} - (0.818 \pm .028)\hat{k},$$

where the letters used to denote the unit vectors correspond to the prong designations.

The interpretation that occurs immediately is

$$_{\Lambda}H^4 \longrightarrow \pi^- + He^3 + n,$$

where the pion caused track C and He^3 caused track B. However, this leads to

$$B_{\Lambda} = -3.4 \pm 1.0 \text{ Mev}$$

TABLE 23

DATA FOR EVENT H3

Track	Length	Remarks
A	11 μm	Originates in at-rest kaon star.
B	20.7 $\pm$ 2.8 μm	
C	19.15 $\pm$ .45 mm	Ends in absorption star having one short prong and a low-energy electron track.

and is therefore unacceptable. The assumption that particle B was more massive than He^3 would only make matters worse since it would lead to larger momentum imbalance and thus larger kinetic energy for the neutron in schemes of the type

$$\Lambda^A \rightarrow \pi^- + B + n.$$

The next simplest type of interpretation involves production of an additional, charged nuclear fragment which did not have enough kinetic energy to generate an observable prong. For an interpretation of this type to be tenable, the residual momentum of particles B and C must be small. Values of the residual momentum were computed for various assumed identities of particle B; they are:

P_R = 55 Mev/c for B = proton

P_R = 30.4 $\pm$ 6.5 Mev/c for B = deuteron

P_R = 16.9 $\pm$ 8.9 Mev/c for B = triton

P_R = 65 Mev/c for B = He^3

P_R = 92 Mev/c for B = He^4.

Clearly, the preferred choice is a triton, although it is conceivable that a deuteron could yield consistency.

Under the assumption that particle B was a deuteron, the schemes

$$_{\Lambda}Li^{8} \rightarrow \pi^{-} + H^{2} + Li^{6}$$
$$_{\Lambda}Li^{9} \rightarrow \pi^{-} + H^{2} + Li^{7}$$
$$_{\Lambda}Li^{10} \rightarrow \pi^{-} + H^{2} + Li^{8}$$
$$_{\Lambda}Be^{11} \rightarrow \pi^{-} + H^{2} + Be^{9}$$
$$_{\Lambda}B^{12} \rightarrow \pi^{-} + H^{2} + B^{10}$$
$$_{\Lambda}B^{13} \rightarrow \pi^{-} + H^{2} + B^{11}$$

were examined. All of these led to unreasonable values for the lambda binding energy. For all schemes (with $B = H^{2}$) involving less massive constituents, the additional charged secondaries should have been observable. It became apparent while making these calculations that schemes involving more massive constituents than those considered would lead to negative values of the lambda binding energy.

Under the assumption that particle B was a triton, the schemes

$$_{\Lambda}H^{4} \rightarrow \pi^{-} + H^{3} + p$$
$$_{\Lambda}He^{6} \rightarrow \pi^{-} + H^{3} + He^{3}$$
$$_{\Lambda}He^{7} \rightarrow \pi^{-} + H^{3} + He^{4}$$
$$_{\Lambda}Li^{9} \rightarrow \pi^{-} + H^{3} + Li^{6}$$
$$_{\Lambda}Li^{10} \rightarrow \pi^{-} + H^{3} + Li^{7}$$
$$_{\Lambda}Be^{10} \rightarrow \pi^{-} + H^{3} + Be^{7}$$
$$_{\Lambda}B^{11} \rightarrow \pi^{-} + H^{3} + B^{7}$$

$$_{\Lambda}B^{13} \rightarrow \pi^- + H^3 + B^{10}$$

were examined. All but two of these led to unreasonable binding energies and any schemes (with B = H^3) involving more massive constituents would do likewise. Two possible interpretations of the event are then

$$_{\Lambda}H^4 \rightarrow \pi^- + H^3 + p$$

$$B_{\Lambda} = 1.75 \pm .61 \text{ Mev}$$

and

$$_{\Lambda}Li^{10} \rightarrow \pi^- + H^3 + Li^7$$

$$B_{\Lambda} = 4.82 \pm .75 \text{ Mev.}$$

The first of these is preferred since the lambda binding energy for the second should be about 7 Mev.[1]

Event H4

The decay resulted in two colinear product prongs. Some of the data are given in Tables 17 and 18 of Chapter III. There, the primary track has been labelled C and the two product prongs have been called track a and track b. The two products were emitted colinearly. The dip angle for track a is + $73^{\circ} \pm 2^{\circ}$ and that for track b is $-70^{\circ} \pm 1^{\circ}$. The focal plane projections of the product prongs were seen to be colinear by inspection.

It has already been argued in Chapter III that track C must have been caused by a hypernucleus. In order to limit

---

[1] Levi-Setti, Slater, and Telegdi, op. cit.

the hypernucleus identity as much as possible, delta-rays were counted along track C; only one was seen. Among the multiply-charged hypernuclei, $_{\Lambda}He^{7}$ yields the lowest expected number[1] of delta-rays, i.e., $4.4\ ^{+3.2}_{-2.0}$. Therefore, particle C was most probably $_{\Lambda}H^{3}$ or $_{\Lambda}H^{4}$. The results of measurements made on tracks a and b are consistent with either of the interpretations

$$_{\Lambda}H^{3} \longrightarrow \pi^{-} + He^{3}$$
$$_{\Lambda}H^{4} \longrightarrow \pi^{-} + He^{4} .$$

The expected range for the nuclei is about 8.5 μm in both instances. This number is consistent with the measured range of 9.1 ± 1.4 μm for track a. The expected pion ranges are about 25 mm for the first and about 39 mm for the second. Both of these are greater than the range, 19.47 mm, which particle b traversed before leaving the stack. Track b dips so steeply that it is impossible to choose between the two interpretations.

Event H5

The hypernucleus originated in an at-rest kaon absorption star. A reproduction of the event is shown in Fig. 1, where the labelling of the tracks is also indicated. The hypernucleus generated track A. Tracks B and D stop with no visible evidence of decay or interaction; track π leaves the emulsion stack; and the particle responsible for track C stopped in the stack and caused an absorption star having

---

[1] Barkas and Young, op. cit.

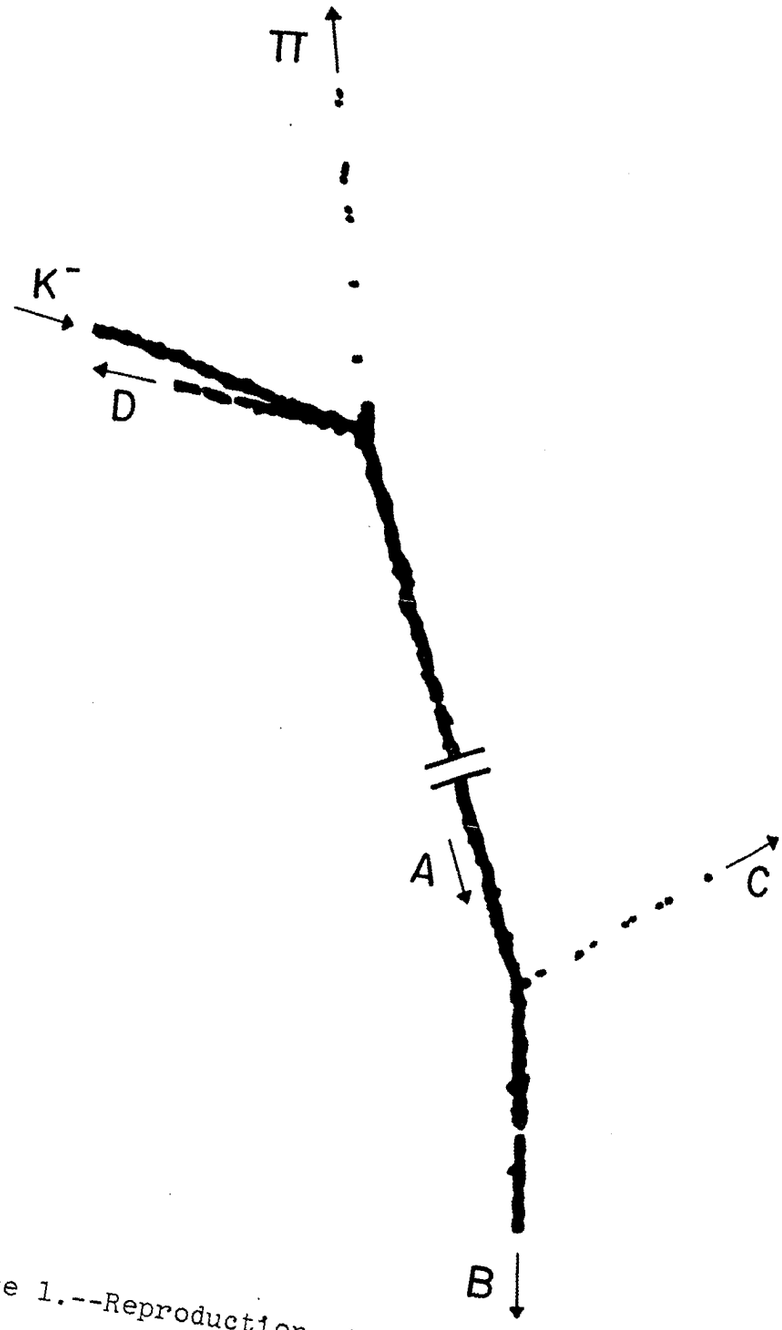

Figure 1.--Reproduction of event H5.

two product prongs, one of length 7 μm and the other of length 9 μm. Track lengths and direction cosines of associated momenta with respect to a conveniently chosen cartesian coordinate system are given in Table 24.

TABLE 24

TRACK LENGTHS AND DIRECTION COSINES OF MOMENTA FOR EVENT H5

Track	Length	Direction Cosines x	y	z
A	157 ± 1.2 μm	1	0	0
B	354 ± 2.4 μm	$0.969 \pm .006$	$-0.243 \pm .030$	$0.050 \pm .014$
C	$31.46 \pm .20$ mm	$-0.515 \pm .010$	$0.857 \pm .006$	0
K^-	$\sim$110 mm			
D	$\sim$450 μm			
π	>72 mm			

The coordinate system pertinent to Table 24 is defined as follows: The x-axis is parallel to track A and directed toward the bottom of the page in Fig. 1; the x-y plane is defined by the plane of tracks A and C and the y-axis is directed toward the right in Fig. 1; the z-axis is perpendicular to the plane of tracks A and C and is directed out of the page in Fig. 1. This coordinate system was chosen because the event has all the earmarks of an in-flight hypernucleus decay.

Delta-ray counting was used to set limits on the charge of particle B, and ionization measurements were used to confirm the identity of the primary kaon, to show that the light track originating in the primary star is most probably due to a pion, and to tentatively establish the identity of particle C.

The expected numbers of delta-rays were computed for various assumed identities of particle B; these are given in Table 25. Four delta-rays were counted along the entire length of track B. Comparison of this result with the values listed in Table 25 shows that, with good confidence, the charge of particle B is bounded by $2 \leq Z_B \leq 4$. One delta-ray was counted along track A. This fact and the comparative appearances of tracks A and B are consistent with $Z_A = Z_B - 1$.

As was stated previously, ionization measurements were used to confirm the identity of the primary kaon. The normalized ionization parameter determined at a residual range of 80 mm is $g^* = 1.81$. Comparison of this with the value, $1.93 \pm .11$, expected for a kaon furnishes the desired confirmation.

Great care was exercised in making the ionization measurements on track C. Both α and g_o were determined in each region of emulsion containing a segment of the track upon which blob and gap counts were carried out. Since the mean dip angle of track C in unprocessed emulsion is 32^o, the data were corrected for dip. In order to confirm the validity of

TABLE 25

EXPECTED NUMBER OF DELTA-RAYS FOR VARIOUS ASSUMED IDENTITIES OF PARTICLE B IN EVENT H5

Identity	Expected Number of Delta-Rays[a]
p	$0^{+1.8}_{-0}$
He^3	$1^{+2.3}_{-0.8}$
Li^6	$2^{+2.6}_{-1.3}$
Be^7	$11^{+4.4}_{-3.3}$
Be^{10}	$15^{+5.0}_{-3.8}$
B^8	$29^{+7.5}_{-5.4}$
B^{12}	$19^{+5.4}_{-4.3}$

[a]The limits correspond to the 68 per cent level of confidence.

the dip correction, measurements were made on a kaon track which stopped in emulsion and which had a mean dip angle of 22°. The mass value obtained from this track is $935 \pm 46\ m_e$

which is consistent with the accepted kaon mass of 966 m_e. The corrected data for track C are given in Table 26.

TABLE 26

IONIZATION DATA FOR TRACK C OF EVENT H5

Residual Range in mm	g*
3.160	4.54
4.355	3.53
6.203	3.17
7.231	2.68
9.630	2.37
12.99	2.43
14.78	2.28
17.32	2.09
19.85	1.74
22.77	1.68
24.15	1.41
27.71	1.71
30.01	1.51
31.16	1.47

The results of the measurements made on track C are also shown in Fig. 2, where they appear as points scattered around the straight line labelled "μ". The straight line labelled "K" is a least squares fit of the indicated kaon data points

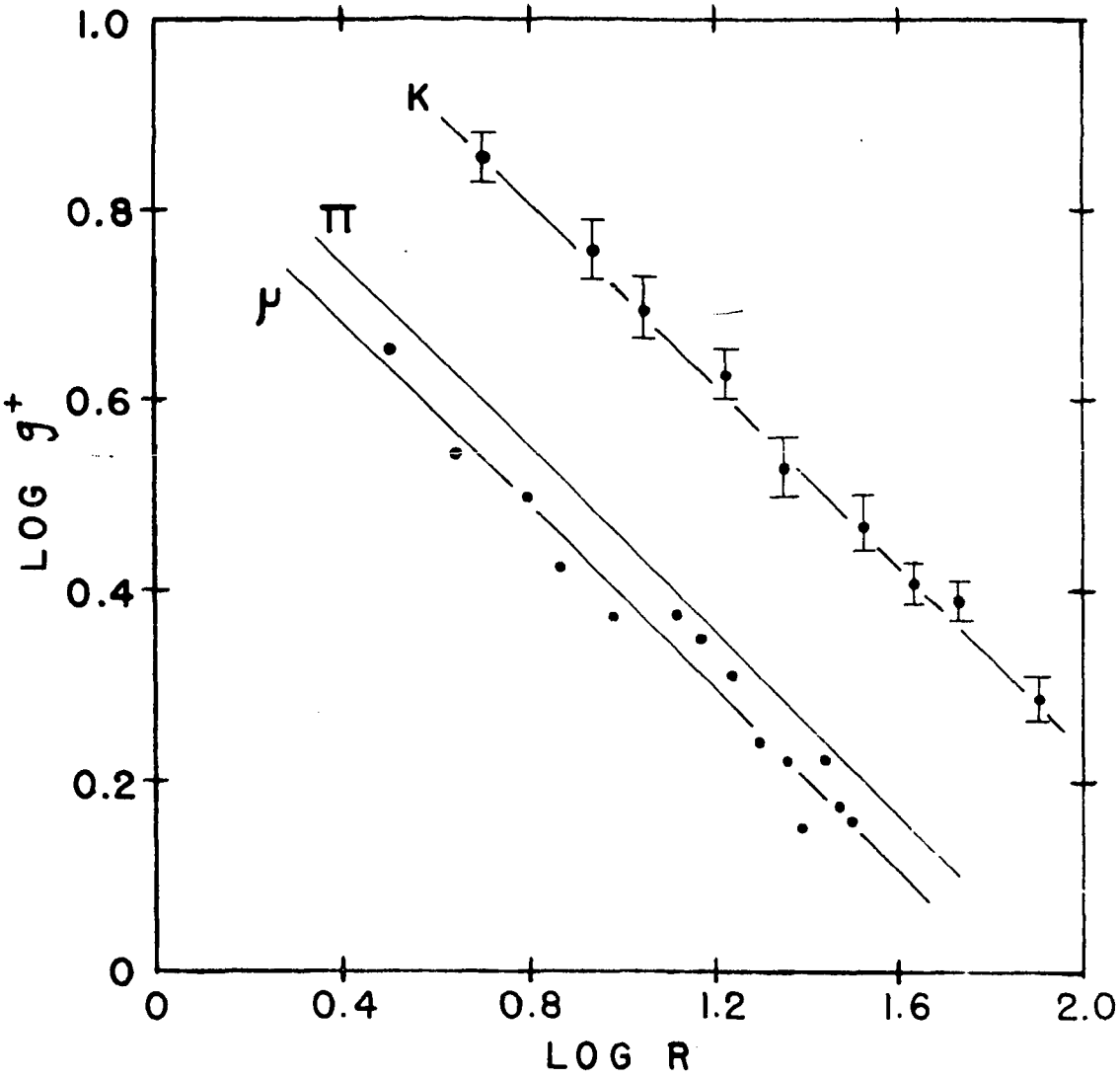

Figure 2.--Results of ionization measurements for track C of event H5.

and those labelled "π" and "μ" are the expected lines for pions and muons, respectively. The latter two have been derived from the kaon measurements and the known mass ratios. It has been shown in Chapter III (see Table 19) that this procedure does not yield reliable results. Because of this, a different method has been used to estimate the mass of particle C.

The measured values of g* (given in Table 19) for two pion tracks were used in making a least-squares fit of the equation

$$\log g^* = - 0.478 \log R + b_{\pi} \ .$$

This gave $b_{\pi} = 0.843 \pm .057$. A glance at Fig. 2 assures one of the approximate validity of assigning the same slopes to kaon and light meson calibration curves. The above equation and the first five entries of Table 26 were used to obtain a mass estimate of $296 \pm 67\ m_e$ for particle C. The mass of the charged pion is $273\ m_e$ and that of the muon is $207\ m_e$. It follows that track C was probably caused by a negative pion.

The residual range of the light track which originates in the primary star cannot be measured since it leaves the emulsion stack before stopping; even so, ionization measurements made on this track can be used to argue that it could not have been caused by an electron or a proton. The results of these measurements are given in Table 27.

TABLE 27

RESULTS OF IONIZATION MEASUREMENTS MADE ON LIGHT TRACK WHICH ORIGINATES IN PRIMARY STAR OF EVENT H5

g*	Distance from Star
1.13	13 mm
1.32	56 mm
1.40	67 mm

These data show that the ionization density increases with distance from the star and that before it leaves the stack the track has ionization density considerably larger than the plateau value. If the track were due to an electron, one would expect it to exhibit a great deal of scattering for an ionization density as large as g* = 1.40. The track shows no apparent scattering so it cannot be due to an electron. The Q-value of the reaction

$$K^- + (2p) \longrightarrow \Lambda + p$$

is 316 Mev. Therefore, a proton cannot be emitted from an at-rest kaon-nucleus interaction with a kinetic energy larger than this value. A proton with this maximum kinetic energy would have a residual range of about 210 mm. The corresponding expected value of g*, derived from the kaon calibration and the known mass ratio, is 1.68. Even though the extension of the measured kaon curve to other types of particles has been demonstrated to be unreliable, it is felt that the magnitude

of the discrepancy could not be large enough to rationalize the difference between g* = 1.68 and the first datum of Table 27.

The only reasonable alternative remaining is that the light track was caused by a pion. Then, the residual range and kinetic energy of the pion at emission were, respectively, 96 ± 13 mm and 95 ± 8.4 Mev. The residual range was determined from the last datum of Table 27 and the (measured!) pion calibration.

The Q-value of

$$K^- + n \longrightarrow \Lambda + \pi^-$$

is 177 Mev, so the pion kinetic energy at emission is consistent with this reaction. The Q-value of

$$K^- + n \longrightarrow \Sigma^\circ + \pi^-$$

is 106 Mev. The kinetic energy of particle D was at least 9 Mev at emission and whatever caused track A must have had a kinetic energy of a few Mev. Also, the binding energy difference before and after the reaction must have amounted to several Mev. After addition of these energies to the pion kinetic energy, it seems difficult to reconcile the energy release from the primary kaon absorption with any reactions other than those in which a charged pion and a lambda hyperon are produced.

These considerations lead to the conclusion that track A could have been caused only by a hypernucleus. One further limiting condition can be derived at this point, i.e.,

the charge of the hypernucleus, Z_A, can be bounded. If track D is that of a proton its kinetic energy at emission was 9 Mev. Then the directly observable kinetic energy, exclusive of that of the hypernucleus, released from the primary kaon absorption is greater than 104 ± 8.4 Mev. If one assumes that the hypernucleus had $Z_A \geq 5$ then 10 Mev is a conservative estimate of a lower bound for the difference between the binding energy of the nucleus which absorbed the kaon and the sum of the binding energies of the reaction products. The sign of this difference in binding energies is such that it acts to decrease the upper bound for the hypernucleus kinetic energy at emission. The maximum possible Q-value for a negative kaon-nucleon reaction in which a charged pion and a lambda hyperon are produced is 177 Mev. Therefore, the kinetic energy of the hypernucleus at emission must have been less than 63 ± 8.4 Mev if $Z_A \geq 5$ was indeed the case. The kinetic energy of a ${}_{\Lambda}B^9$ having a residual range of 157 μm (length of track A) is 77 Mev. One concludes that $1 \leq Z_A \leq 4$.

Possible Interpretations for the Hypernucleus Decay

According to the direction cosines given in Table 24, tracks A, B, and C are not coplanar. There is, however, some indication that particle A underwent a small-angle scatter just before the decay point, and the measured deviation from coplanarity is small. Thus, it is possible that the direction measurements are misleading and that tracks

A, B, and C may indeed have been coplanar very near the decay vertex.

If any interpretations involving the emission of one or more neutral particles can be shown to be consistent with the measurements, then they will be preferred. Those interpretations which appear most likely at this stage of the development belong to the class

$$\Lambda^{A} \longrightarrow B + \pi^{-} + \text{(one or more neutrons)}. \qquad \text{I}$$

It is possible (although unlikely) that one or more charged secondaries, unobservable by reason of insufficient energy, may have been emitted. Accordingly, interpretations belonging to the class

$$\Lambda^{A} \longrightarrow B + \pi^{-} + \text{nucleons (free or bound)} \ (Z_B \leq Z_A) \qquad \text{II}$$

should also be examined in detail. Finally, the possibility of a radiative decay of the bound lambda must be admitted. Hyperons are expected to undergo radiative decay with branching ratios of the order of 0.1 per cent--4 per cent on the basis of current theory.[1] Two events which support this expectation have been reported. The most likely interpretation of one of these[2] is

$$\Sigma^{+} \longrightarrow n + \pi^{+} + \gamma$$

---

[1] S. Barshay and R. E. Behrends, Phys. Rev. 114, 931 (1959).

[2] E. M. Friedlander, Phys. Rev. Lett. 4, 528 (1960).

and of the other[1] is

$$\Sigma^- \rightarrow n + \pi^- + \gamma \ ,$$

where γ is a photon. Radiative hypernucleus decays which are of interest here belong to the class

$$_{\Lambda}^{A} \rightarrow B + \pi^- + \gamma \ . \qquad \text{III}$$

Before beginning detailed analyses of the previously delimited interpretations, one generally useful piece of information can be extracted from the measurements, i.e., the momentum at emission of the decay pion can be determined. This momentum is 122.30 $\pm$ .55 Mev/c.

In order to carry out a detailed consistency check for a particular hypernucleus decay scheme, one must know the mass of the hypernucleus involved. Many hypernucleus masses in the range $1 \leq Z \leq 4$ have been measured directly,[2] but there are a few possible hypernuclei whose charges lie within this range and whose existence is at least plausible ($_{\Lambda}Li^{6}$, for example) which, to the best of the author's knowledge, have not yet been observed. For these as yet unobserved hypernuclei, the best one can do is to make reasonable estimates of the masses, based on the measured hyperon binding energies for similar hypernuclei. The hypernucleus masses used in this work are given in Appendix III.

---

[1] M. Nikolic, et al., Nuclear Phys. 15, 519 (1960).

[2] Levi-Setti, Slater, and Telegdi, op. cit.

Analysis of the One-Neutron Decay Modes

Those schemes belonging to class I in which only one neutron is emitted will be considered first since these are most simply dealt with and thus lead to a convenient presentation of methods. It is desirable at this point to introduce the following notation:

P_A = Momentum of hypernucleus at decay

E_A = Total energy of hypernucleus at decay

P_{Bx} = x-component of momentum of fragment B at emission

P_{By} = y-component of momentum of fragment B at emission

P_{Bz} = z-component of momentum of fragment B at emission

E_B = Total energy of fragment B at emission

P_{Cx} = x-component of momentum of particle C at emission

P_{Cy} = y-component of momentum of particle C at emission

P_{Cz} = z-component of momentum of particle C at emission

E_C = Total energy of particle C at emission

M_A = Mass of hypernucleus

M = Mass of neutron

P_{nx} = x-component of neutron momentum at emission

P_{ny} = y-component of neutron momentum at emission

P_{nz} = z-component of neutron momentum at emission

E_n = Total energy of neutron at emission.

The coordinate system defined in the discussion of Table 24 will be used in this section.

Momentum conservation leads to

$$P_A = P_{Bx} + P_{Cx} + P_{nx} \qquad (5\text{-}1)$$

$$0 = P_{By} + P_{Cy} + P_{ny} \qquad (5\text{-}2)$$

$$0 = P_{Bz} + P_{nz} \, . \qquad (5\text{-}3)$$

Substitutions of the definitions

$$P_x = P_{Bx} + P_{Cx}$$

$$P_y = P_{By} + P_{Cy}$$

$$P_z = P_{Bz}$$

into equations (5-1), (5-2), and (5-3) give

$$P_{nx} = P_A - P_x \qquad (5\text{-}4)$$

$$P_{ny} = -P_y \qquad (5\text{-}5)$$

$$P_{nz} = -P_z \, . \qquad (5\text{-}6)$$

Total energy conservation is expressed by

$$E_A = E_B + E_C + E_n \, ,$$

or, equivalently, by

$$\left[P_A^2 + M_A^2\right]^{1/2} = E + \left[(P_A - P_x)^2 + P_y^2 + P_z^2 + M^2\right]^{1/2} , \qquad (5\text{-}7)$$

where $E = E_B + E_C$, E is expressed in Mev (Bev), momenta are expressed in Mev/c (Bev/c), and masses in Mev/c^2 (Bev/c^2). All quantities which appear in equation (5-7), with the exception of P_A, are determined once one has chosen a particular hypernucleus decay scheme. This equation thus determines P_A, provided a real solution exists. An algebraic solution may be obtained simply by squaring twice and performing a certain amount of manipulation. This algebraic solution is

$$P_A = \frac{1}{2(E^2-P_x^2)} \left\{ P_x(M_A^2 + E^2 - Q^2) \pm E \left[(M_A^2 + Q^2 - E^2)^2 - 4M_A^2 (Q^2 - P_x^2) \right]^{1/2} \right\} , \qquad (5\text{-}8)$$

where $Q^2 = M^2 + P_x^2 + P_y^2 + P_z^2$. Equation (5-8) is also the algebraic solution of the equation

$$E_A = E - E_n , \qquad (5\text{-}9)$$

since the sign of E_n is lost when equation (5-7) is squared a second time. However, if one looks at the magnitudes of the quantities involved, then it becomes clear that no real solution of equation (5-9) can exist under the conditions appropriate to this event. An analogous statement holds for all other schemes belonging to class I and for all schemes belonging to class II. Just the converse holds true for class III schemes so these must be treated in a different manner. Whether or not real solutions exist for equation (5-7) may be determined simply by evaluating the discriminant,

$$D = (M_A^2 + Q^2 - E^2)^2 - 4M_A^2 (Q^2 - P_x^2) , \qquad (5\text{-}10)$$

which appears in equation (5-8). The existence of a real solution is implied by $D \geq 0$ and $D < 0$ implies that P_A is a complex number. The latter alternative is physically inadmissible.

If charge conservation and baryon conservation are invoked, then it is easy to enumerate the one-neutron schemes which are consistent with $1 \leq Z_A \leq 4$, $2 \leq Z_B \leq 4$, and

secondary fragment stability requirements. These are

$$\Lambda^{H^4} \longrightarrow He^3 + \pi^- + n$$
$$\Lambda^{He^7} \longrightarrow Li^6 + \pi^- + n$$
$$\Lambda^{Li^8} \longrightarrow Be^7 + \pi^- + n$$
$$\Lambda^{Li^{10}} \longrightarrow Be^9 + \pi^- + n.$$

In order for the discriminant, D, to be greater than or equal to zero for any of these schemes it is necessary that the pion momentum be less than 89 Mev/c. It is not apparent from the form of D that $\frac{\partial D}{\partial P_C} < 0$ for, say,

$85 \text{ Mev/c} \leq P_C \leq 195 \text{ Mev/c}$, nor is this apparent even from the explicit expression that one gets for $\frac{\partial D}{\partial P_C}$; however, one can assure himself that this is indeed so by numerical evaluations of $\frac{\partial D}{\partial P_C}$ for a few selected schemes. A detailed treatment of this point will be deferred until all class I and class II schemes have been discussed.

The physical reason for the kinematical inconsistencies discussed above is that the decay products have just too much kinetic energy. The mass of the hypernucleus is, of course, larger than that of any of the decay products so that if things are arranged to conserve momentum then the total energy of the decay products is always greater than that of the hypernucleus. One can see this analytically by evaluating

$$\Delta = E_A - E - E_n \qquad (5\text{-}11)$$

for a conveniently chosen value of P_A, e.g., for $P_A = 0$. The

fact that equation (5-7) has only complex roots implies that Δ has the same sign for all real values of P_A. An examination of Δ at $P_A = 0$ for the various one-neutron schemes quickly shows that $\Delta < 0$ provided that $P_C \geq 89$ Mev/c.

Analysis of the Multineutron Schemes

The remaining schemes which belong to class I are

$$_{\Lambda}Li^{9} \longrightarrow Be^{7} + \pi^{-} + 2n$$

$$_{\Lambda}Li^{10} \longrightarrow Be^{7} + \pi^{-} + 3n.$$

P_A is not uniquely determined by momentum and energy conservation requirements for these schemes since there are more variables than equations. The discussion of multineutron schemes is thus not so simple as the discussion of one-neutron schemes. It is convenient to prove a lemma as a prelude to this more complicated discussion.

Assume that n particles, all having non-zero rest mass, are emitted from a decay in such a manner that their total momentum is fixed. It will be shown that their total energy is then a minimum if they are all emitted together, i.e., if they all have precisely the same velocity. Let the x, y, and z components of momentum and the mass of the i^{th} emitted particle be denoted by P_{ix}, P_{iy}, P_{iz}, and M_i, respectively. The function

$$\sum_{i=1}^{n} E_i = \sum_{i=1}^{n} (P_{ix}^2 + P_{iy}^2 + P_{iz}^2 + M_1^2)^{1/2} ,$$

where E_i is the total energy of the i^{th} emitted particle, must be minimized subject to the side conditions

$$\sum_{i=1}^{n} P_{ix} - G_x = 0 \qquad (5\text{-}12)$$

$$\sum_{i=1}^{n} P_{iy} - G_y = 0 \qquad (5\text{-}13)$$

$$\sum_{i=1}^{n} P_{iz} - G_z = 0, \qquad (5\text{-}14)$$

where the x, y, and z components of the fixed momentum are G_x, G_y, and G_z, respectively. Application of the method of Lagrange multipliers yields

$$\frac{P_{ix}}{E_i} + \lambda_1 = 0 \qquad 1 \leq i \leq n \qquad (5\text{-}15)$$

$$\frac{P_{iy}}{E_i} + \lambda_2 = 0 \qquad 1 \leq i \leq n \qquad (5\text{-}16)$$

$$\frac{P_{iz}}{E_i} + \lambda_3 = 0 \qquad 1 \leq i \leq n, \qquad (5\text{-}17)$$

where λ_1, λ_2, and λ_3 are Lagrange multipliers which are constants independent of particle index. A bit of manipulation of equations (5-15), (5-16), and (5-17) gives

$$\frac{P_{ix}^2 + P_{iy}^2 + P_{iz}^2}{E_i^2} = \lambda_1^2 + \lambda_2^2 + \lambda_3^2 \qquad 1 \leq i \leq n$$

or

$$\frac{P_i^2}{E_i^2} = \lambda_1^2 + \lambda_2^2 + \lambda_3^2 \qquad 1 \leq i \leq n, \qquad (5\text{-}18)$$

where P_i is the total momentum of the i^{th} particle. In the unit system implicit here, P_i and E_i are related by

$$P_i = \beta_i E_i , \qquad (5\text{-}19)$$

where β_i has the usual meaning. Substitution of equation (5-19) into (5-18) yields

$$\beta_i^2 = \lambda_1^2 + \lambda_2^2 + \lambda_3^2 \qquad 1 \leq i \leq n. \qquad (5\text{-}20)$$

The right-hand side of equation (5-20) is a constant independent of particle index; therefore, all of the particles have the same speed at emission if their total energy is the minimum value consistent with a fixed total momentum. Equations (5-15), (5-16), and (5-17), together with equation (5-18), imply

$$\frac{P_{ix}}{P_i} + \frac{\lambda_1}{\lambda} = 0 \qquad 1 \leq i \leq n \tag{5-21}$$

$$\frac{P_{iy}}{P_i} + \frac{\lambda_2}{\lambda} = 0 \qquad 1 \leq i \leq n \tag{5-22}$$

$$\frac{P_{iz}}{P_i} + \frac{\lambda_3}{\lambda} = 0 \qquad 1 \leq i \leq n, \tag{5-23}$$

where

$$\lambda = (\lambda_1^2 + \lambda_2^2 + \lambda_3^2)^{1/2} .$$

Equations (5-21), (5-22), and (5-23) imply that all of the particles are emitted with parallel momenta.[1] The previously obtained solution cannot correspond to the maximum total energy at emission because this would be realized by giving the total fixed momentum to a single particle whose mass is equal to the smallest member of the set $\{M_i\}$.

If the multineutron schemes can be shown kinematically inconsistent by reason of too much total energy of the decay products even when all the neutrons are emitted together, then the preceding lemma implies that these schemes are kinematically inconsistent for any choice of momenta of the neutrons. Consistency for the minimum energy configuration

---

[1]The author is indebted to Professor R. A. Howard for supplying this proof.

of neutron momenta may be checked simply by evaluating the discriminant defined by equation (5-10) wherein M has been replaced by the sum of the masses of all emitted neutrons. Again, for both multineutron schemes, the discriminant is negative for pion momenta greater than or equal to 89 Mev/c, and it is easy to see that the quantity Δ, defined by equation (5-11), is negative for $P_A = 0$ and $P_C \geq 89$ Mev/c.

Analysis of Class II Schemes

These schemes involve the emission of one or more nucleons or nuclear fragments additional to fragment B, at least one of which is charged but unobservable because of insufficient energy. There are very many such schemes consistent with charge conservation, baryon conservation, $1 \leq Z_A \leq 4$, and $2 \leq Z_B \leq 4$. Fortunately, it turns out that detailed consistency checks are necessary for only a limited number of them. Exactly the same methods may be used here as were used for the multineutron schemes; one has only to replace M by the sum of the masses of all nucleons or fragments, additional to fragment B, which were emitted from the hypernucleus decay. It is useful to examine $\frac{\partial D}{\partial Q^2}$. Differentiation of the appropriately modified discriminant originally defined by equation (5-10) yields

$$\frac{\partial D}{\partial Q^2} = Q^2 - E^2 - 2M_A^2 . \qquad (5\text{-}24)$$

A brief examination of the quantities involved assures one that $\frac{\partial D}{\partial Q^2} < 0$. Once the identities of the hypernucleus and fragment B have been specified, the total baryon number and charge number of possible additional nucleons are uniquely determined. The only freedom of choice remaining is then the specification of the way in which the additional nucleons are bound. From the manner in which Q^2 has been defined, it is apparent that Q^2 assumes its minimum value when the additional nucleons are combined in such a way that their total binding energy has the maximum value consistent with stability requirements. If a scheme for particular choices of hypernucleus and fragment B identities and for the additional nucleons combined to give maximum binding energy can be shown inconsistent then all other possible combinations of nucleons additional to fragment B will lead to kinematically inconsistent schemes. This fact permits one to check all class II schemes by detailed examinations of only a limited number of all those possible. Those which must be analyzed are listed in Appendix IV.

The methods developed in connection with the analysis of multineutron schemes have been used to show that all but a few of the class II schemes are absolutely inconsistent for pion momenta greater than 97 Mev/c. The exceptional ones are

$$_{\Lambda}Li^{8} \longrightarrow He^{4} + \pi^{-} + He_{o}^{4}$$

$$_{\Lambda}Li^{10} \longrightarrow He^{4} + \pi^{-} + He_{o}^{6}$$

$$_{\Lambda}Li^{10} \longrightarrow He^{6} + \pi^{-} + He_{o}^{4}$$

$$_{\Lambda}Li^{9} \longrightarrow He^{4} + \pi^{-} + n + He_{o}^{4}$$

$$_{\Lambda}Li^{10} \longrightarrow He^{4} + \pi^{-} + 2n + He_{o}^{4} \quad ,$$

where the subscript "o" indicates that the corresponding fragment is unobservable. A glance at the preceding list shows that in every instance at least one of the decay products is an alpha particle. This may be understood by recalling that the binding fraction for the alpha particle is anomalously large compared to those for other light nuclei. It is convenient to subdivide the exceptional schemes into those having no neutral decay products and those for which at least one of the decay products is a neutron.

The discussion of those having no neutral decay products will be carried out first. For these, the momentum of the hypernucleus is uniquely determined by equation (5-8) wherein the neutron mass, M, must be replaced by M_o, the mass of the unobservable charged fragment. The x, y, and z components of momentum of the unobserved fragment are, respectively, given by

$$P_{ox} = P_A - P_x \qquad (5\text{-}25)$$

$$P_{oy} = -P_y \qquad (5\text{-}26)$$

$$P_{oz} = -P_z \; . \qquad (5\text{-}27)$$

The criterion for fragment unobservability has been taken to be the requirement that its range in emulsion must have been less than or equal to 2 μm. This criterion allows one to establish an upper bound for the momentum of the unobservable fragment and, in turn, to bound the momentum difference $P_A - P_x$. This difference may be determined by evaluating equation (5-8). In order for the unobservability criterion to be satisfied for any of the first three exceptional schemes, the pion momentum must have been less than 100 Mev/c. During the course of making these calculations it became apparent that for none of these three schemes could the momentum of the unobservable secondary have been parallel to the direction of track A or that of track B.

A different approach must be used to analyze the last two exceptional schemes since P_A is not uniquely determined for these. The unobservability criteria in this case must also admit the possibility of track coincidence. If the (assumed!) track of the unobservable secondary is not coincident with either track A or track B then it has been required that its length be less than or equal to 2 μm. If the assumed track is coincident with either track A or track B near the decay vertex, its length has been required to be less than or equal to 20 μm. For non-coincidence of tracks, the treatment has been carried out as though all quantities other than the momentum and energy of the neutron(s) were determined. One may establish an upper bound for the

discriminant, D, by putting

$$E = E_B + E_C + M_o \tag{5-28}$$

$$P_y = 0 \tag{5-29}$$

$$P_z = 0 \tag{5-30}$$

$$P_x = P_{Bx} + P_{Cx} + P_o \ , \tag{5-31}$$

where M_o is the mass of the unobserved charged secondary and P_o is its momentum at a residual range of 2 μm. For track coincidence, one again proceeds as though all quantities other than the momentum and energy of the neutron(s) were determined. In this case, however, an upper bound for D is established by putting

$$E = E_B + E_C + E_o \tag{5-32}$$

$$P_y = P_{By} + P_{Cy} + P_{oy} \tag{5-33}$$

$$P_z = P_{Bz} + P_{oz} \tag{5-34}$$

$$P_x = P_{Bx} + P_{Cx} + P_{ox} \ , \tag{5-35}$$

where E_o, P_{ox}, P_{oy}, and P_{oz} are, respectively, total energy and x, y, and z components of momentum of the unobservable charged secondary. The momentum components can be determined because the directions of tracks A and B are known. Calculations were carried out for several values of residual range between 0 and 20 μm. The results of these calculations show that, in order for the unobservability criteria to be satisfied for any of the exceptional class II schemes, the pion momentum at emission would necessarily have been less

than 100 Mev/c at emission.

During the discussion of the one-neutron schemes, it was stated that it would be demonstrated that $\frac{\partial D}{\partial P_C} < 0$ for 85 Mev/c $\leq P_C \leq$ 195 Mev/c by numerical evaluations for a few selected class I and class II schemes. The relevant expression is

$$\frac{1}{4} \frac{\partial D}{\partial P_C} = (M_A^2 + Q^2 - E^2)\left(\alpha P_x + \beta P_y - \frac{E P_C}{E_C} \right) - 2M_A^2 \beta P_y \quad , \tag{5-36}$$

where α and β are, respectively, the x and y direction cosines of the momentum of Particle C. The results of these calculations are presented in Table 28; during the course of making the calculations it became apparent that $\frac{\partial D}{\partial P_C} < 0$ for all class I and II schemes.

Analysis of Class III Schemes

The necessity of admitting the possibility of radiative hypernucleus decay has already been pointed out. Schemes belonging to class III and consistent with $1 \leq Z_A \leq 4$, $2 \leq Z_B \leq 4$, charge conservation, baryon conservation, and secondary fragment stability requirements are

TABLE 28

VALUES OF $\frac{1}{4}\frac{\partial D}{\partial P_C}$ FOR SELECTED CLASS I AND II INTERPRETATIONS OF EVENT H5

Decay Scheme	Pion Momentum in Mev/c	$\frac{1}{4}\frac{\partial D}{\partial P_C}$ in $(Bev)^3$
$\Lambda^{H^4} \rightarrow He^3 + \pi^- + n$	85	- 12.37
	195	- 19.74
$\Lambda^{Li^{10}} \rightarrow Be^9 + \pi^- + n$	85	- 59.37
	195	-118.22
$\Lambda^{Li^{10}} \rightarrow He^3 + \pi^- + n + He^6$	85	-216.73
	195	-331.56

$$\Lambda^{H^3} \rightarrow He^3 + \pi^- + \gamma$$
$$\Lambda^{H^4} \rightarrow He^4 + \pi^- + \gamma$$
$$\Lambda^{He^6} \rightarrow Li^6 + \pi^- + \gamma$$
$$\Lambda^{He^7} \rightarrow Li^7 + \pi^- + \gamma$$
$$\Lambda^{Li^7} \rightarrow Be^7 + \pi^- + \gamma$$
$$\Lambda^{Li^9} \rightarrow Be^9 + \pi^- + \gamma$$
$$\Lambda^{Li^{10}} \rightarrow Be^{10} + \pi^- + \gamma \ .$$

For these schemes, momentum conservation leads to

$$E_\gamma = \left[(P_A - P_x)^2 + P_y^2 + P_z^2\right]^{1/2} , \qquad (5\text{-}37)$$

where E_γ is the energy of the emitted photon.

It was pointed out earlier that the previously employed method of checking kinematical consistency is inappropriate for use in connection with class III schemes because real

solutions of the equation

$$E_A = E - E_\gamma \qquad (5\text{-}38)$$

exist for some of these schemes when 85 Mev/c $\leq P_C \leq$ 195 Mev/c. Even though one knows that these solutions are physically inadmissible, the validity of the method is still voided by their mere existence. It is therefore necessary to devise a method of checking consistency in which the signs of square roots are carried through explicitly.

Assume the decay scheme

$$\Lambda^A \longrightarrow B + \pi^- + X,$$

where X is a neutral particle having rest mass M which may be either zero or finite. Then, with the notation used in connection with the one-neutron schemes, define a quantity $P_{Ao} > 0$ by

$$\left[P_{Ao}^2 + M_A^2\right]^{1/2} = E + \left[P_y^2 + P_z^2 + M^2\right]^{1/2} . \qquad (5\text{-}39)$$

Assume that $P_{Ao} > P_x$, i.e., $P_{Ao} - P_x > 0$. Then, in order for kinematical consistency to prevail, a solution, $P > 0$, must exist for

$$\left[(P_{Ao} + P)^2 + M_A^2\right]^{1/2} = E + \left[(P_{Ao} + P - P_x)^2 + E_o^2\right]^{1/2}, \qquad (5\text{-}40)$$

where

$$E_o^2 = P_y^2 + P_z^2 + M^2 . \qquad (5\text{-}41)$$

Rephrased, equation (5-40) is

$$E_A(P) = E + E_X(P), \tag{5-42}$$

where E_X is the total energy of the neutral particle and E_A and E_X are looked upon as functions of the variable, P, defined by equation (5-40). Equivalent to the solution of equation (5-40) is the solution, $P > 0$, of

$$\int_0^P \left[\frac{dE_A(S)}{dS} - \frac{dE_X(S)}{dS}\right] dS + E_A(S = 0) - E_X(S = 0) = E. \tag{5-43}$$

Equation (5-43) may be rewritten to give

$$\int_0^P \left[\frac{dE_A}{dS} - \frac{dE_X}{dS}\right] dS = E + \left[(P_{Ao} - P_X)^2 + E_o^2\right]^{1/2} - \left[P_{Ao}^2 + M_A^2\right]^{1/2}. \tag{5-44}$$

It is apparent from the definition of P_{Ao} and the assumption $P_{Ao} - P_X > 0$ that the right-hand side of equation (5-44) is a positive quantity. This fact implies that

$$\int_0^P J(S)dS > 0, \tag{5-I1}$$

where

$$J(S) = \frac{dE_A}{dS} - \frac{dE_X}{dS} \quad . \tag{5-45}$$

Differentiation of E_A and E_X yields

$$J(S) = \frac{P_{Ao} + S}{\left[(P_{Ao} + S)^2 + M_A^2\right]^{1/2}}$$

$$- \frac{P_{Ao} + S - P_x}{\left[(P_{Ao} + S - P_x)^2 + E_o^2\right]^{1/2}} \quad . \tag{5-46}$$

It is necessary to examine the asymptotic behavior of J(S). As $S \rightarrow \pm \infty$, then

$$J(S) \rightarrow \frac{1}{2S^2} (E_o^2 - M_A^2) ,$$

or

$$J(S) \rightarrow \begin{cases} - \dfrac{\left|E_o^2 - M_A^2\right|}{2S^2} & \text{for } M_A > E_o \\ + \dfrac{\left|E_o^2 - M_A^2\right|}{2S^2} & \text{for } M_A < E_o \end{cases} \quad .$$

Only the first of these two alternatives is of interest here so it is clear that J(S) is negative for very large values of $|S|$. The zeros of J(S) are also needed. These are given by the solutions of

$$\frac{(P_{Ao} + S)\left[(P_{Ao} + S - P_x)^2 + E_o^2\right]^{1/2}}{E_A(S)\,E_X(S)} =$$

$$\frac{(P_{Ao} + S - P_x)\left[(P_{Ao} + S)^2 + M_A^2\right]^{1/2}}{E_A(S)\,E_X(S)}$$

or, since E_A and E_X are positive, by the solutions of

$$(P_{Ao} + S)^2\left[(P_{Ao} + S - P_x)^2 + E_o^2\right] =$$

$$(P_{Ao} + S - P_x)^2\left[(P_{Ao} + S)^2 + M_A^2\right] . \qquad (5\text{-}47)$$

These roots are

$$S_1 = \frac{P_x M_A}{M_A + E_o} - P_{Ao} \qquad (5\text{-}48)$$

$$S_2 = \frac{P_x M_A}{M_A - E_o} - P_{Ao} . \qquad (5\text{-}49)$$

It is apparent from equations (5-48) and (5-49) that $S_1 < S_2$ if $P_x > 0$. The latter inequality is satisfied for all possible interpretations of the event being considered. The assumption $P_{Ao} > P_x$ implies $S_1 < 0$.

The general forms which J(S) may assume are now apparent. These are represented schematically in Fig. 3. A glance at Fig. 3 shows that a solution of equation (5-44) can exist only if $S_2 > 0$. Thus a necessary condition for kinematical consistency when $M_A > E_o$ and $P_{Ao} > P_x$ is

$$P_x > P_{Ao}\left[\frac{M_A - E_o}{M_A}\right] . \qquad (5\text{-}I2)$$

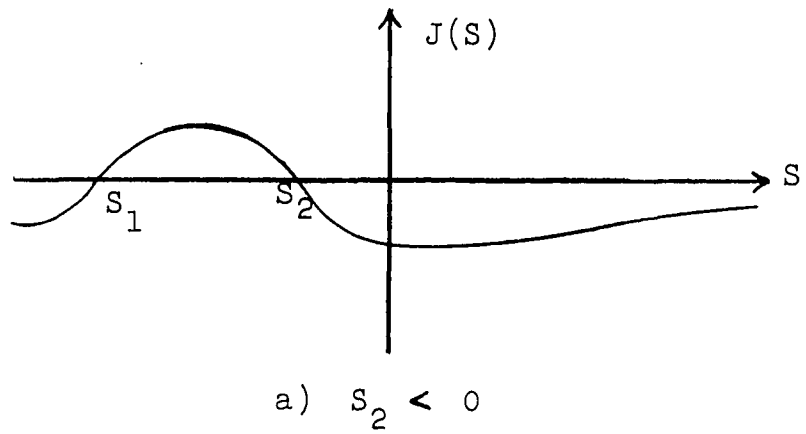

a) $S_2 < 0$

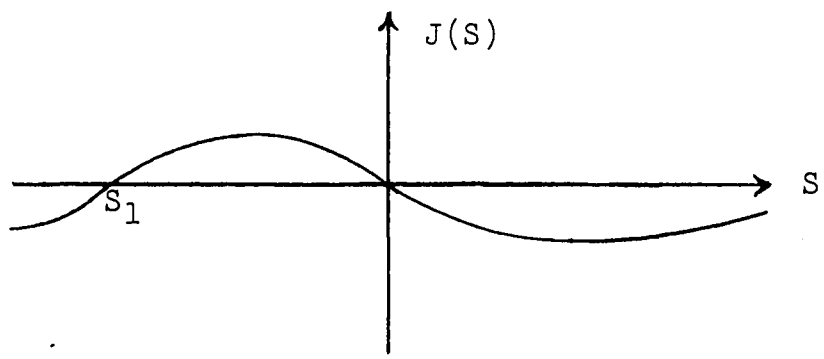

b) $S_2 = 0$

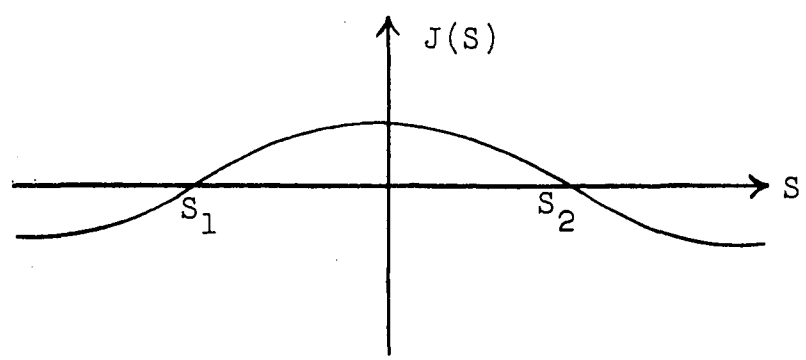

c) $S_2 > 0$

Figure 3.--Schematic representation of the form of the function J(S).

Necessary and sufficient conditions for kinematical consistency are $S_2 > 0$ and

$$\int_0^{S_2} J(S)\, dS \geq E + \left[(P_{Ao} - P_x)^2 + E_o^2\right]^{1/2} - \left[P_{Ao}^2 + M_A^2\right]^{1/2} . \qquad (5\text{-I3})$$

Evaluation of the left-hand side of inequality (5-I3) at the limits of integration yields

$$(M_A - E_o)\left[1 + \frac{P_x^2}{(M_A - E_o)^2}\right]^{1/2} \geq E. \qquad (5\text{-I4})$$

It is apparent from the left-hand side of this inequality that the proper signs for the square roots have indeed been carried explicitly through the development. Furthermore, it is impossible that the inequality

$$(E_o - M_A)\left[1 + \frac{P_x^2}{(M_A - E_o)^2}\right]^{1/2} \geq E$$

be satisfied in the present context so

$$(M_A - E_o)^2\left[1 + \frac{P_x^2}{(M_A - E_o)^2}\right] \geq E^2 \qquad (5\text{-I5})$$

is precisely the same statement as inequality (5-I4). Rewriting inequality (5-I5) gives

$$(M_A - E_o)^2 + P_x^2 - E^2 \geq 0. \qquad (5\text{-I6})$$

This inequality constitutes a necessary and sufficient condition for kinematical consistency when $P_x > 0$, $P_{Ao} > P_x$, and $M_A > E_o$. That it is necessary is apparent. It is sufficient because the integral which appears on the left-hand side of equation (5-44) is a continuous function of its upper limit and because the satisfaction of inequality (5-I6) implies that $S_2 > 0$ and thus that inequality (5-I2) is satisfied.

It follows that sufficient conditions for kinematical inconsistency are

$$P_{Ao} > P_x \tag{5-I7}$$

$$E^2 - (M_A - E_o)^2 - P_x^2 > 0. \tag{5-I8}$$

Inequality (5-I7) may be reformulated by using

$$P_{Ao}^2 = (E + E_o)^2 - M_A^2 . \tag{5-50}$$

The result of this operation is

$$(E + E_o)^2 - M_A^2 - P_x^2 > 0. \tag{5-I9}$$

It is useful to notice that satisfaction of

$$E^2 - M_A^2 - P_x^2 > 0 \tag{5-I10}$$

implies satisfaction of both inequalities (5-I8) and (5-I9).

The consistency check for each class III scheme was carried out by evaluating I_1, I_2, and I_3--which are defined to be the left-hand sides of inequalities (5-I8), (5-I9), and (5-I10), respectively--for several values of pion momentum

between 85 Mev/c and 195 Mev/c. The utility of evaluating I_3 is made apparent by examining

$$\frac{\partial I_3}{\partial P_C} = 2E \frac{P_C}{E_C} - 2P_x \frac{\partial P_x}{\partial P_C} \quad . \tag{5-51}$$

For all class III schemes and 85 Mev/c $\leq P_C \leq$ 195 Mev/c, $P_x > 0$ and $\frac{\partial P_x}{\partial P_C} < 0$. These imply

$$\frac{\partial I_3}{\partial P_C} > 0 \quad . \tag{5-III}$$

Therefore, if $I_3 > 0$ for a particular value of P_C then it is unnecessary to carry out evaluations for larger values of P_C. The results of these calculations show that all class III schemes are kinematically inconsistent for 85 Mev/c $\leq P_C \leq$ 195 Mev/c.

It is worth mentioning that one need not consider photon emission in connection with any class I or class II scheme because the minimum decay product energy would be given by zero photon energy.

Final Interpretation of Event H5

It has now been established that none of the class I, II, and III schemes are consistent with the measurements. When the ionization measurements were made on track C, the unreliability of the derived pion and muon log g* vs. log R curves had not yet been discovered. Thus, it was first

believed that particle C was a muon and that the most likely interpretations of the event involved the muon decay of a bound lambda. This hypothesis is untenable in view of the mass value obtained for particle C by means of the measured pion curve.

The only remaining alternative is that the event was a pionic two-body, in-flight decay of a hypernucleus. The only identities of fragment B which yield momentum conservation are He^3 and He^4. The interpretation

$$ {}_{\Lambda}H^3 \rightarrow He^3 + \pi^- $$

leads to a lambda binding energy of about -14 Mev and is therefore physically inadmissible. One is left with the unique interpretation

$$ {}_{\Lambda}H^4 \rightarrow He^4 + \pi^- , $$

where the decay occurred while the hypernucleus was in flight. At emission, the kinetic energy and momentum of the pion were, respectively, $45.99 \pm .36$ Mev and $122.30 \pm .55$ Mev/c. The alpha-particle had a kinetic energy of $30.24 \pm .31$ Mev and a momentum of 475.7 ± 2.5 Mev/c. The residual momentum transverse to track A is 10.8 ± 14.4 Mev/c and is therefore consistent with conservation of momentum. The hypernucleus had a momentum of 398.9 ± 4.0 Mev/c at the decay point; this leads to a proper time of flight of 4.7×10^{-12} sec. for the hypernucleus. Finally, the lambda binding energy was

$$ B_{\Lambda} = 1.48 \pm .68 \text{ Mev.} $$

The Mean Life of $_{\Lambda}H^{4}$

Because the times of flight of hypernuclei observed in emulsions are usually short compared to the mean life of the free lambda, in-flight hypernucleus decays are rarely observed. A consequence of this is the fact that hypernucleus mean lives are known only in a very rough way.

The decay

$$_{\Lambda}H^{4} \rightarrow He^{4} + \pi^{-}$$

is ideally suited for a more precise determination of the mean life of the bound lambda for two reasons: (1) there is no chance of confusion between in-flight and at-rest decays, (2) this decay is among those most often observed. Since event H5 is an in-flight example of this decay, it was decided to make a survey of the literature and compute the mean life of $_{\Lambda}H^{4}$ from the results of the survey.

A total of four in-flight decays have been found and sixty-three at-rest decays were included in the analysis. The in-flight decays were taken from the following sources: (1) Levi-Setti, Slater, and Telegdi[1]--one event, (2) Filipkowski, et al.[2]--one event, (3) Deka[3]--one event, (4) this dissertation--one event. The at-rest decays were taken from:

---

[1] Levi-Setti, Slater, and Telegdi, op. cit.

[2] A. Filipkowski, et al., Nuclear Phys. 7, 643 (1958).

[3] G. C. Deka, Nuovo Cimento 14, 1217 (1959).

(1) Levi-Setti, Slater, and Telegdi[1]--10 events, (2) Deka[2]--one event, (3) Ekspong, et al.[3]--one event, (4) Nora and Ortalli[4]--one event, (5) EFINS-NU collaboration[5]--49 events, (6) this dissertation--one event.

The method of maximum likelihood[6] shows that the most probable mean life is given by the sum over all events of the hypernuclei times of flight divided by the total number of in-flight decays. This procedure yields

$$t = 3.5^{+\,3.2}_{-\,1.5} \times 10^{-10} \text{ sec.},$$

where t is the mean life of ${}_{\Lambda}H^{4}$ and the deviations correspond to a 68 per cent level of confidence. This number is in agreement with the mean life of the free lambda, which is $3.0 \pm .2 \times 10^{-10}$ sec.

---

[1] Levi-Setti, Slater, and Telegdi, op. cit.

[2] Deka, op. cit.

[3] A. G. Ekspong, et al., Phys. Rev. Lett. 3, 103 (1959).

[4] S. Nora and I. Ortalli, Nuovo Cimento 12, 635 (1959).

[5] Private communication from Dr. O. Skjeggestad, The Enrico Fermi Institute for Nuclear Studies, University of Chicago.

[6] See, e.g., Franzinetti and Morpurgo, op. cit.

CHAPTER VI

SUMMARY

Nearly three hundred negative kaon tracks were followed to their terminations in an emulsion stack. The endings of these tracks were segregated as to type (in-flight interaction, in-flight decay, at-rest interaction), and some easily accessible characteristics of negative kaon-nucleus interactions have been determined.

These determined characteristics are in general agreement with results obtained by other workers. One exception exists, i.e., the observed emission frequencies of charged pions, from both at-rest and in-flight interactions resulting in at least one charged product, are slightly larger than any which have been reported in the literature. This disagreement may be attributed to a difference in scanning efficiencies.

One event, interpreted as

$$K^- + \text{Nucleus} \longrightarrow \pi^- + \Sigma^- + \text{Nucleons},$$

was seen. Up to now, whether or not simultaneous π^- and Σ^- production occurs in kaon-nucleus interactions has been an unsettled question.

Some simple scattering measurements were made for 183 of the kaon tracks. The results of these measurements indicate the existence of two components of the kaon beam in the energy interval 92 Mev to 112 Mev. One component apparently underwent more scattering than the other. It must be emphasized that the statistical reliability of the measurements is rather poor, so these results can be taken only as an indication of anomalous behaviour. If real, the anomaly could originate in the existence of two different kinds of negative kaons. An alternative, but less appealing, hypothesis is that the kaon may exist in one or more excited states.

Detailed analyses have been carried out for five hypernucleus events. Four of these originated in kaon-nucleus interactions and one in the nuclear absorption of a negative sigma hyperon. The interpretations of two $_{\Lambda}H^{4}$ events, one of which was an in-flight decay, are unique. For two other hypernucleus events, the charge was uniquely determined, but in both cases two adjacent mass numbers yield consistency with the observations. For the remaining event, the interpretation given is highly probable but depends upon the assumed emission of a particle unobserved by reason of insufficient energy. All of the lambda binding energies obtained are in good agreement with the expected values.

Finally, the mean life of $_{\Lambda}H^{4}$ was calculated by using the combined results of this dissertation and a literature survey. The value obtained is $3.5^{+3.2}_{-1.5} \times 10^{-10}$ sec. This number is in agreement with the mean life of the free lambda hyperon.

BIBLIOGRAPHY

Books

Bennett, C. A. and Franklin, N. L. Statistical Analysis in Chemistry and the Chemical Industry. New York: John Wiley and Sons, 1954.

Dalitz, R. H. Reports on Progress in Physics. London: The Physical Society, 1957. Vol. 20, p. 163.

Kendall, M. G. The Advanced Theory of Statistics. Vol. 2 New York: Hafner Publishing Co., 1951.

Molina, E. C. Poisson's Exponential Binomial Limit. New York: D. Van Nostrand Co., 1942.

Voyvodic, L. "Particle Identification with Photographic Emulsions, and Related Problems," Progress in Cosmic Ray Physics. Vol. II. ed. J. G. Wilson. New York: Interscience Publishers, 1954.

Reports

Barkas, W. H., Nuovo Cimento 8, 201 (1958).

Barkas, Walter H. and Young, D. M., University of California Radiation Laboratory Report UCRL-2579 Rev., September, 1954 (unpublished).

Barshay, S. and Behrends, R. E., Phys. Rev. 114, 931 (1959).

Beasley, C. O., Jr. and Holladay, W. G., Suppl. Nuovo Cimento 7, 77 (1958).

Beiser, A., Revs. Modern Phys. 24, 273 (1952).

Deka, G. C., Nuovo Cimento 14, 1217 (1959).

Eisenberg, Y., et al., Nuovo Cimento 8, 663 (1958).

Eisenberg, Y., et al., Nuovo Cimento 9, 745 (1958).

Eisenberg, et al., Nuovo Cimento 11, 351 (1959).

Ekspong, A. G., et al., Phys. Rev. Lett. 3, 103 (1959).

Filipkowski, A., et al., Nuclear Phys. 7, 643 (1958).

Fowler, P. H. and Perkins, D. H., Phil. Mag. 46, 587 (1955).

Franzinetti, C. and Morpurgo, G., Suppl. Nuovo Cimento 6, 469 (1957).

Friedlander, E. M., Phys. Rev. Lett. 4, 528 (1960).

Gell-Mann, M., Phys. Rev. 92, 833 (1953).

Gurney, R. W. and Mott, N. F., Proc. Roy. Soc. 164A, 150 (1938).

K^--Collaboration, Part I, Nuovo Cimento 13, 690 (1959).

K^--Collaboration, Part II, Nuovo Cimento 14, 315 (1959).

K^--Collaboration, Part III, Nuovo Cimento 15, 873 (1959).

Koch, W., et al., Helv. Phys. Acta 3, 237 (1960).

Levi-Setti, R., Slater, W. E., and Telegdi, V. L., Suppl. Nuovo Cimento 10, 68 (1958).

Lodge, J., et al., Nuovo Cimento 18, 147 (1960).

Lohrmann, E., et al., Nuovo Cimento 7, 163 (1958).

Nakano, T. and Nishijima, K., Progr. Theoret. Phys. (Kyoto) 10, 581 (1953).

Nikolic, M., et al., Helv. Phys. Acta 3, 221 (1960).

Nikolic, M., et al., Nuclear Phys. 15, 519 (1960).

Nora, S. and Ortalli, I., Nuovo Cimento 12, 635 (1959).

O'Ceallaigh, C., CERN Report, B.S. 11, 1954 (unpublished).

Tidman, D. A., George, E. P., and Herz, A. J., Proc. Phys. Soc. A 66, 1019 (1953).

APPENDICES

APPENDIX I

PELLICLE PROCESSING

The first step after exposure of the stack is to mount each pellicle on a glass plate. At this time, the thickness of each pellicle should be measured and each of them should be numbered according to order in the stack (a sharpened pencil or similar instrument may be used to inscribe the number). Each pellicle should be immersed completely in a gelatin solution together with a glass plate and the two joined after making certain that no air bubbles cling to either of the contact surfaces. The joined pellicle and glass plate are then removed from the solution and a weighted roller run over the emulsion surface to insure that no vacancies exist between the contact surfaces. The mounted emulsions should be stored in a dark place until dry. The gelatin solution should be prepared as follows:

1. Dissolve 60 gm of gelatin powder in 1 liter of distilled water.
2. Allow to stand overnight. This will result in a semi-solid gelatin.
3. Add 3 liters of distilled water.

4. Dissolve gelatin at 50°C.

5. Cool to 30° C.

6. Filter the solution (use vacuum filter flask).

7. Add 40 cc of glycerine and 4 cc of wetting agent.

8. Cool to 23°C before using.

After drying, the emulsions are ready to be developed. The developer recipe is:

35 gm boric acid.

18 gm sodium sulfite.

0.8 gm potassium bromide.

1 liter distilled water.

Add 4.5 gm amidol and 4 cc wetting agent immediately before use.

The stop bath consists of one part acetic acid and two hundred parts distilled water (by volume). The fixer recipe is:

1 liter distilled water.

4000 gm sodium thiosulfate (hypo).

5.6 gm sodium bisulfite.

0.5 gm silver nitrate.

If some previously used, undiluted fixer is available, one part of this should be combined with five parts of fresh fixer prepared without the addition of the silver nitrate. A suggested schedule for development is:

Time	Bath	Temperature
9:30 - 12:00	Distilled water	$25^{\circ}C \rightarrow 5^{\circ}C$
12:00 - 14:30	Developer	$5^{\circ}C$
14:30 - 14:50	Dry	$5^{\circ}C \rightarrow 25^{\circ}C$
14:50 - 15:50	Dry	$25^{\circ}C$
15:50 - 16:10	Dry	$25^{\circ}C \rightarrow 5^{\circ}C$
16:10 - 18:40	Stop bath	$5^{\circ}C$
18:40	Fixer	$5^{\circ}C$

Fixation with undiluted fixer should continue for about 20 to 24 hours for emulsions which are 600 microns thick. Thereafter the fixer should be gradually diluted. Say there were originally 60 parts undiluted fixer, then a suggested dilution schedule is:

Time	Parts Fixer Removed	Parts Distilled Water Added
Monday, 5 P.M.	10	5
10 P.M.	-	5
Tuesday, 8 A.M.	12	6
12 A.M.	-	6
4 P.M.	15	7
8 P.M.	-	8
Wednesday, 8 A.M.	12	12
11 A.M.	12	12
2 P.M.	12	12
5 P.M.	12	12
8 P.M.	Start tap water and continue until emulsions are clear.	

All solutions should be filtered before use and the fixer solution should be circulated continuously.

Bubbles occasionally form during the fixation and clearing stage. One fairly successful technique for removal of these is to use a hypodermic needle and syringe (without plunger) connected to a vacuum pump.

After clearing, the emulsions should be placed on an accurately level surface and allowed to dry. The emulsions should, incidentally, be maintained in an accurately level position throughout the processing. It is better if the drying occurs gradually.

This procedure usually results in a surface silver deposit. It may be removed with soft cotton and ethanol after the emulsions are dry. One must do this quite carefully to avoid scratching the surfaces.

APPENDIX II

THE COORDINATE METHOD OF COMPUTING TRACK LENGTHS

This is most simply explained through reference to an illustration.

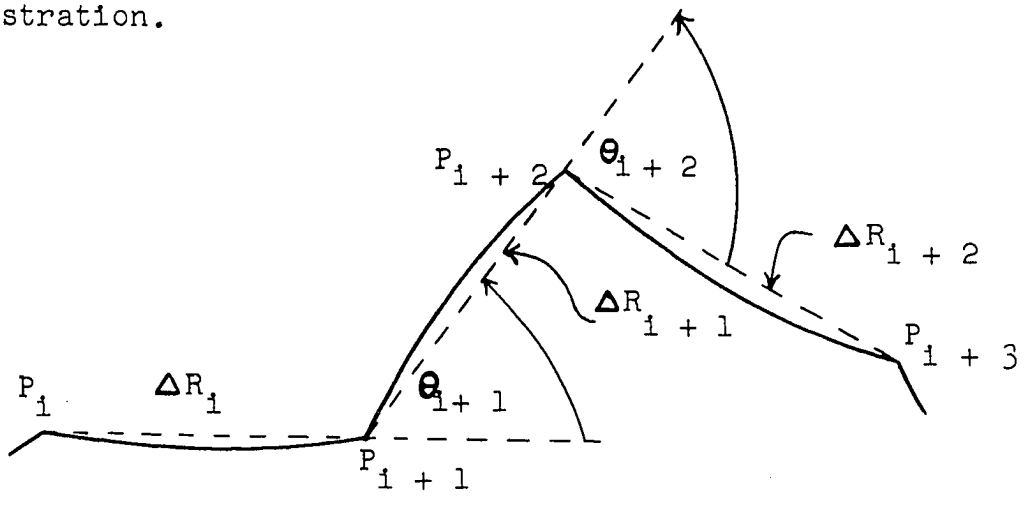

Figure 4.--Schematic illustration of the coordinate method of computing track lengths. The heavy, continuous curve represents a track segment; its curvature is greatly exaggerated for purposes of clarity.

In this method, the (cartesian) coordinates of all points where an apparent change in track direction occurs are recorded. Such points are represented by P_i, P_{i+1}, P_{i+2}, and P_{i+3} in Figure 4. The track length is then given to a good approximation by the sum of the chord lengths between successive coordinate points. In the example of Figure 4 the length of the track segment between points

P_i and P_{i+3} would be approximated by

$$\Delta R = \Delta R_i + \Delta R_{i+1} + \Delta R_{i+2} ,$$

where the length of a particular chord is given by

$$\Delta R_i = \left[(x_{i+1} - x_i)^2 + (y_{i+1} - y_i)^2 + k^2 (z_{i+1} - z_i)^2 \right]^{1/2} .$$

The shrinkage factor, k, that appears in the preceding expression is defined by

$$k = \frac{\text{emulsion thickness before processing}}{\text{apparent thickness after processing}} ,$$

where the thicknesses are, in both instances, measured at the same place in the emulsion. The apparent thickness after processing is given by the difference between the fine focusing motion readings at the top and bottom of the emulsion, and z-coordinates are always measured in units of the drum divisions for the microscope fine focusing motion. The apparent depth in emulsion depends upon the relative index of refraction at the top surface of the emulsion. This effect is automatically compensated by the use of the same combination of optics for measurements of track coordinates and shrinkage factor determinations and by the way in which the shrinkage factor has been defined. The nominal shrinkage factor determined in this way for emulsions 24 through 49 is $2.075 \pm .046$. This value is quoted only in order to indicate the precision of the method. The shrinkage factors are sensitive to room humidity and depend specifically upon

the linkage of the microscope fine focusing motion. The x and y coordinates were measured with Ames dial indicators reading directly in microns and which had been calibrated with the standard stage micrometer.

The calculations which must be carried out to get at the track lengths can become quite tedious, particularly for long tracks. In order to shorten this labor, the relevant calculations have been programmed for an IBM 650 computer. This program facilitates computation of the quantities listed in Table 29.

TABLE 29

QUANTITIES COMPUTED WITH AID OF TRACK LENGTH PROGRAM

Quantity	Word Number[a]
ΔR_i	2
$\sum_{n=1}^{i} \Delta R_n$	3
$\sum_{n=1}^{i} \frac{k(z_{n+1} - z_n)^2}{\Delta R_n}$	4
ΔR_{i-1}	5
$\cos \theta_{i-1}$	6
$\sin \theta_{i-1}$	7

TABLE 29--Concluded

Quantity	Word Number[a]
$\sum_{n=1}^{i-1} \sin \theta_n$	8

[a]The word number corresponds to the quantity location on the output card.

The notation of Figure 4 has been used throughout and the segment number, i, is given in word 1 of each output card--there is one output card for each track segment. One data input card is used for each recorded coordinate point; the x, y, and z coordinates are entered in words 1, 2, and 3, respectively, and when the coordinate point is that of the entrance of a track in a new emulsion or that just after translation of the origin of one of the indicators, the appropriate shrinkage factor, k, is entered in word 4. In the assembly of the input data deck, a transfer card ($+0000000010^{+}7$ entered in word 1) must immediately precede each data card having an entry in word 4. Provision is made for inclusion of indicator calibrations; the x and y indicator calibrations (in microns per indicator division) are stored in drum locations 0300 and 0301, respectively. The appropriate 650 console settings are as follows:

Storage Entry switches--70 1951 9999

Control switch--RUN

Display switch--Arbitrary

Half cycle switch--RUN

Programmed Stop switch--STOP

Overflow switch--STOP

Error switch--STOP.

The Master Subroutine control panel must be used, and the calculations are carried out with machine floating point arithmetic.

The utility of most of the quantities appearing in Table 29 is apparent. The quantity corresponding to Word 4 deserves clarification, however. This quantity is just

$$\frac{\partial}{\partial k} \sum_{n=1}^{i} \Delta R_n = \sum_{n=1}^{i} \frac{k(z_{n+1} - z_n)^2}{\Delta R_n}$$

and is useful in estimating probable errors. Almost all uncertainty in the final track length is due to fluctuations in the measured shrinkage factors so other sources of uncertainty may be neglected by comparison. The quantity corresponding to word 8 should also be explained. It was felt that this might prove useful as a measure of scattering in instances where only low precision is required.

APPENDIX III

TABLE OF HYPERNUCLEUS MASSES

Hypernucleus	Mass in Bev/c^2
Λ^{H^3}	2.991
Λ^{H^4}	3.924
Λ^{He^4}	3.924
Λ^{He^5}	4.842
Λ^{He^6}	5.779[a]
Λ^{He^7}	6.716[a]
Λ^{Li^6}	5.781[a]
Λ^{Li^7}	6.712
Λ^{Li^8}	7.643
Λ^{Li^9}	8.581[a]
$\Lambda^{Li^{10}}$	9.516[a]
Λ^{Be^7}	6.706[a]
Λ^{Be^8}	7.644
Λ^{Be^9}	8.562
$\Lambda^{Be^{10}}$	9.501[a]
$\Lambda^{Be^{11}}$	10.434[a]

[a]Mass has been estimated.

APPENDIX IV

CLASS II HYPERNUCLEUS DECAY SCHEMES ANALYZED IN DETAIL FOR EVENT H5

In the following decays, the subscript "o" implies unobservability of the corresponding object and d and t are, respectively, deuteron and triton.

$$_{\Lambda}He^{4} \longrightarrow He^{3} + \pi^{-} + p_{o}$$

$$_{\Lambda}He^{5} \longrightarrow He^{3} + \pi^{-} + d_{o}$$

$$\longrightarrow He^{4} + \pi^{-} + p_{o}$$

$$_{\Lambda}He^{6} \longrightarrow He^{3} + \pi^{-} + t_{o}$$

$$\longrightarrow He^{4} + \pi^{-} + d_{o}$$

$$_{\Lambda}He^{7} \longrightarrow He^{3} + \pi^{-} + n + t_{o}$$

$$\longrightarrow He^{4} + \pi^{-} + t_{o}$$

$$\longrightarrow He^{6} + \pi^{-} + p_{o}$$

$$_{\Lambda}Li^{6} \longrightarrow He^{3} + \pi^{-} + He^{3}_{o}$$

$$\longrightarrow He^{4} + \pi^{-} + 2p_{o}$$

$$_{\Lambda}Li^{7} \longrightarrow He^{3} + \pi^{-} + He^{4}_{o}$$

$$\longrightarrow He^{4} + \pi^{-} + He^{3}_{o}$$

$$\longrightarrow Li^{6} + \pi^{-} + p_{o}$$

$$_{\Lambda}Li^{8} \rightarrow He^{3} + \pi^{-} + n + He_{o}^{4}$$
$$\rightarrow He^{4} + \pi^{-} + He_{o}^{4}$$
$$\rightarrow He^{4} + \pi^{-} + n + He_{o}^{3}$$
$$\rightarrow He^{6} + \pi^{-} + 2p_{o}$$
$$\rightarrow Li^{6} + \pi^{-} + d_{o}$$
$$\rightarrow Li^{7} + \pi^{-} + p_{o}$$
$$_{\Lambda}Li^{9} \rightarrow He^{3} + \pi^{-} + He_{o}^{6}$$
$$\rightarrow He^{4} + \pi^{-} + n + He_{o}^{4}$$
$$\rightarrow He^{4} + \pi^{-} + 2n + He_{o}^{3}$$
$$\rightarrow He^{6} + \pi^{-} + He_{o}^{3}$$
$$\rightarrow Li^{6} + \pi^{-} + t_{o}$$
$$\rightarrow Li^{7} + \pi^{-} + d_{o}$$
$$\rightarrow Li^{8} + \pi^{-} + p_{o}$$
$$_{\Lambda}Li^{10} \rightarrow He^{3} + \pi^{-} + n + He_{o}^{6}$$
$$\rightarrow He^{4} + \pi^{-} + He_{o}^{6}$$
$$\rightarrow He^{4} + \pi^{-} + 2n + He_{o}^{4}$$
$$\rightarrow He^{4} + \pi^{-} + 3n + He_{o}^{3}$$
$$\rightarrow He^{6} + \pi^{-} + He_{o}^{4}$$
$$\rightarrow He^{6} + \pi^{-} + n + He_{o}^{3}$$
$$\rightarrow Li^{6} + \pi^{-} + n + t_{o}$$
$$\rightarrow Li^{7} + \pi^{-} + t_{o}$$
$$\rightarrow Li^{8} + \pi^{-} + d_{o}$$
$$\rightarrow Li^{9} + \pi^{-} + p_{o}$$

$$\Lambda^{Be^7} \longrightarrow He^3 + \pi^- + d_o + 2p_o$$
$$\longrightarrow He^4 + \pi^- + 3p_o$$
$$\Lambda^{Be^8} \longrightarrow He^3 + \pi^- + t_o + 2p_o$$
$$\longrightarrow He^4 + \pi^- + d_o + 2p_o$$
$$\longrightarrow Li^6 + \pi^- + 2p_o$$
$$\longrightarrow Be^7 + \pi^- + p_o$$
$$\Lambda^{Be^9} \longrightarrow He^3 + \pi^- + Li^6_o$$
$$\longrightarrow He^4 + \pi^- + t_o + 2p_o$$
$$\longrightarrow He^6 + \pi^- + 3p_o$$
$$\longrightarrow Li^6 + \pi^- + He^3_o$$
$$\longrightarrow Li^7 + \pi^- + 2p_o$$
$$\longrightarrow Be^7 + \pi^- + d_o$$
$$\Lambda^{Be^{10}} \longrightarrow He^3 + \pi^- + Li^7_o$$
$$\longrightarrow He^4 + \pi^- + Li^6_o$$
$$\longrightarrow He^6 + \pi^- + d_o + 2p_o$$
$$\longrightarrow Li^6 + \pi^- + He^4_o$$
$$\longrightarrow Li^7 + \pi^- + He^3_o$$
$$\longrightarrow Li^8 + \pi^- + 2p_o$$
$$\longrightarrow Be^7 + \pi^- + t_o$$
$$\longrightarrow Be^9 + \pi^- + p_o$$

$$\Lambda Be^{11} \longrightarrow He^{3} + \pi^{-} + Li_{o}^{8}$$

$$\longrightarrow He^{4} + \pi^{-} + Li_{o}^{7}$$

$$\longrightarrow He^{6} + \pi^{-} + t_{o} + 2p_{o}$$

$$\longrightarrow Li^{6} + \pi^{-} + n + He_{o}^{4}$$

$$\longrightarrow Li^{7} + \pi^{-} + He_{o}^{4}$$

$$\longrightarrow Li^{8} + \pi^{-} + He_{o}^{3}$$

$$\longrightarrow Li^{9} + \pi^{-} + 2p_{o}$$

$$\longrightarrow Be^{7} + \pi^{-} + n + t_{o}$$

$$\longrightarrow Be^{9} + \pi^{-} + d_{o}$$

$$\longrightarrow Be^{10} + \pi^{-} + p_{o}$$